Analysis of the Gas Electron Multiplier readout system for the International Linear Collider Time Projection Chamber prototype at DESY

Tuva Richert
Lund University

January 2009 - July 2009

Abstract

In this thesis, I describe the performance analysis of a prototype Time Projection Chamber (TPC) detector with a Gas Electron Multiplier (GEM) readout system. The test beams are available at DESY. There is also a detailed description of the experimental setup and the readout electronics.

A GEM TPC detector is a good candidate for one of the main tracking detectors in the future International Linear Collider experiment, and I discuss the advantages with a GEM based TPC over the more commonly used MWPC (Multi Wire Proportional Chamber). The analysis focuses on the position resolution in the bend plane and the reconstruction of tracks in two dimensions, which is done by a cluster finding algorithm written in C++ within the ROOT analysis framework. The algorithm is described in detail.

The results from the analysis show that two different problems arises due to non parallel magnetic and electric fields, and a second problem probably due to module misalignment. These problems affect the position resolution, and will have to be kept under better control in the future. The position resolution goal for the final TPC is $\sim$100 μm, and the results from these studies shows a spatial resolution of $\sim$120-130 μm.

Contents

1 Introduction

Particle physics uses the Standard Model to describe the basic building blocks of matter and how the elementary particles are bound together by the forces of nature. Experiments can provide convincing support to the Standard Model - which however still is unsatisfactory in many respects, and further experiments are needed - pushing its applicability to its limits. These experiments often involve colliding particles or atomic nuclei at high energies to create new particles or states that can be studied. To perform a collider experiment, an accelerator that accelerates the colliding particles is required. In order to extract the information from the experiment, for example what kind of particles that were created, or what properties the new state had - highly efficient, high resolution detectors and read out systems must be used.

The main topic of this project is the performance analysis of a prototype Time Projection Chamber (TPC) tracking detector, with a novel read out system, GEM (Gas Electron Multiplier), for a development of the main tracking detector in the experiment at the future International Linear Collider (ILC). A test beam for studies of the performance of the prototype TPC is available at DESY, Hamburg. The analysis of the test beam data focuses on track reconstruction and spatial resolution.

2 The International Linear Collider (ILC)

ILC is a future project which involves many countries and research groups. Two opposing, several kilometers long linear accelerators (linacs) based on superconducting acceleration cavities, will collide electrons and positrons at Tera-scale energies to investigate new physics. The ILC project will explore and test the Standard Model of Particle Physics and give answer to fundamental questions and undiscovered principles of nature. A detector system, the Large Detector Concept LDC (which is one of several detector system options for the ILC, where the LDC is of interest here since it will have a TPC as the main tracking detector), will extract information about the collisions. A good candidate for the main tracking detector in LDC is a GEM based TPC.

2.1 Physics motivation for the ILC

The overall physics goal of the ILC is to perform precision experiments at extremely favorable background conditions, not attainable in hadron collisions. Thus, an experimental development for the ILC strives at substantially better momentum resolution than today's experiments. This gives good mass resolution and therefore allow precise measurements. The center of mass energies at the linear collider will have a range between 500 GeV - 1 TeV [8], which is enough to access new processes such as top-quark pair production, the search for particles that constitutes the dark matter, exploring super symmetry (SUSY) and Higgs production [8]. Interesting physics appear in multi-jet final states and the reconstruction of the invariant mass of two or more jets will provide an essential tool for identifying W, Z, Higgs particles and new states or decays [11].

The Higgs boson couples to particles with mass, and would fit in the Standard Model if existing. To create and detect the Higgs particle, high energy is required since the today's limit of the Higgs mass is roughly 200 GeV/c^2 [8]. At ILC, the Higgs search is based on the Higgs strahlung process, $e^+ + e^- \rightarrow Z^{0*} \rightarrow H + Z^0$, where the Z-boson accompanying the Higgs can be used to tag the event by its decay into a lepton pair. If the momentum resolution of the tracking chamber is

good enough, the mass of the recoiling system, i.e. the Higgs candidate, can be determined. Thus, in this way the contribution from all possible decay channels are included in the signal. This is what determines the requirement on momentum resolution and single point resolution for the TPC, and is therefore of special interest for the analysis done in this theses.

At the LHC (Large Hadron Collider), the Higgs boson must be identified through its various decay channels in the presence of a large QCD background. The background limits the number of decay channels that can be used, and LHC is therefore considered a "discovery machine", while the ILC is the "precision machine". Most likely, the final energy choice of the ILC will await indications of the Higgs mass from the first round of LHC experiments.

Since the collisions take place between electrons - not between hadrons as in LHC, the initial interaction is electromagnetic, which makes the analysis much easier since the electromagnetic force is well understood, and that is a clear physics motivation for constructing a lepton collider.

2.2 The accelerator

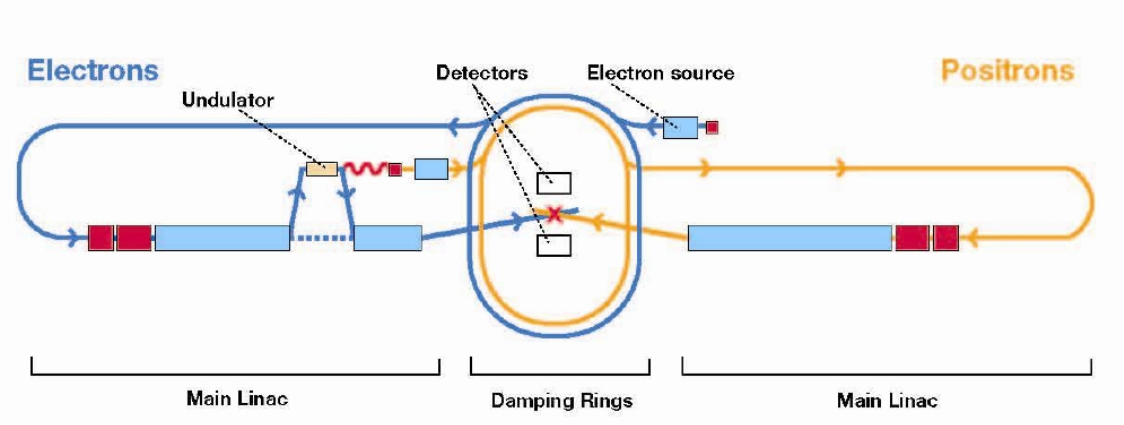

Figure 1: A schematic illustration of the international linear collider accelerator. The two linacs will have a length of approximately 12 km each (depending on energy), and a center of mass energy in the range 500 GeV to 1 TeV.

By letting high intensity light pulses from a laser knock out electrons from a target, the electron beam will be produced[16]. The positron beam will be produced by sending the electron beam through an undulator and thereby produce photons. The photons will then hit a titanium alloy target, giving rise to pair production. The positrons created in the pair production process will be collected and accelerated in the linac[16]. Figure 1 shows the setup schematically.

Particle accelerators use electric fields to accelerate stable charged particles. These electric fields are provided by acceleration cavities; a pair of electrodes over which an oscillating electric field is applied. In the circular machines, the particles pass repeatedly through the same cavities until the final energy is reached. In linear accelerators, the cavities are placed in a row and the final energy is given by the number of cavities and the field strength per meter cavity. In circular accelerators, electric fields of ~ 5 MV/m have been used. Cavities have been developed for the ILC which can produce fields of $\sim$35 MV/m. The length of the linear accelerator is then determined from the final collision energy that is aimed for, and the electric field provided by the cavities.

The acceleration is performed as a standing wave, i.e. the electric field varies as a sine wave (the polarity of the field changes); it has an accelerating period and a decelerating period which forces the particles to come in bunches and not as a continuous beam. During the decelerating period, the bunches must be shielded from the field in drift tubes.

In the ILC conceptual design study, the transverse size of the bunches will be varying over the acceleration period, but will end up as 5 nanometers in the collision point. The bunches will contain $2 \cdot 10^{10}$ electrons and positrons[16], and one bunch train will contain 3000 bunches. The bunches need to be cooled in damping rings to smaller phase space spread before acceleration in the main linacs of the ILC. The damping rings will be housed in a common tunnel at the center of the ILC complex. The beams are focused to extremely small size to get the luminosity of $2 \times 10^{34} cm^{-2} s^{-1}$ [10], which is required for the physics to be studied in the ILC. Several design studies of how ILC will be realized are developed.

2.3 Advantages and disadvantages with a linear collider

In an electron-positron synchrotron (circular accelerator), the beam energy is limited due to the energy loss of the electrons and positrons by the emission of synchrotron radiation. This radiated energy is proportional to the fourth power of the particle gamma factor, and is inversely proportional to the square of the radius of the path. At the LEP (Large Electron Positron) accelerator, with a circumference of 26.67 km, the highest center of mass energy was $\sim$200 GeV. To reach higher energies in a circular electron-positron collider, the circumference must be unreasonable large. A linear collider, as the ILC, has the advantage that the electrons and positrons do not suffer from energy losses due to synchrotron radiation. But to reach 500 GeV - 1 TeV, the linear accelerators still has to be large in size (and thus expensive).

One other advantage with the ILC is that the energy can be varied (or upgraded). The high resolution, compared to e.g. LHC, is also a clear advantage.

A disadvantage with a linear collider is the loss of the non colliding particles. In a circular accelerator, the particles that do not participate in the first collision continues in the accelerator and are used in the following collisions. In a linear collider this is not possible, and the focusing of the beam to extremely small dimensions is crucial for having good enough luminosity.

2.4 The Large Detector Concept (LDC)

The detectors for the ILC are still in an early development and design phase. It is therefore important with simulations and prototype studies such as the ILC TPC prototype at DESY. The TPC detector is a good candidate for the central tracker in one of the options for the ILC detector system, namely the LDC (see figure 2). LDC involves vertex, tracking, calorimeter and muon identifier systems[14]. The detectors will be optimized for reconstruction of individual particles in jets and particle track separation. Vertex detection allows reconstruction of the full vertex topology of the particles produced, which is critical for weak decays. Tracking detectors placed outside the vertex detector provide the momentum for charged particles. These detectors are the topic of this thesis. Calorimeters are used to reconstruct the jet energy and by the calorimeter's hermetic coverage of the collision point, they can provide a total energy measurement, allowing missing energy analysis which is essential in the search for new physics.

Particles which have penetrated the calorimeters without interaction are identified as muons in the muon identification system - the outermost device of the detector system.

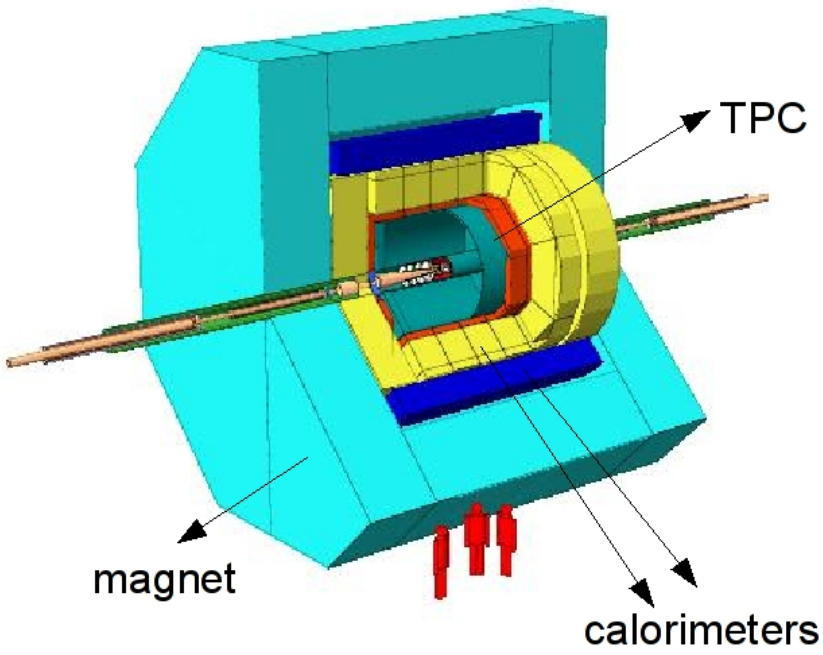

Figure 2: A schematic illustration of the Large Detector Concept. [ref. 11]

3 Time projection chambers

Three dimensional, gaseous tracking detectors can provide track and energy loss information about charged particles traversing the detector and about charged particles in jets created in the collision. A gas filled, cylinder shaped chamber with an applied uniform electric field directed along the cylinder axis constitutes the large drift region. A charged particle from the collision will enter the detector and ionize the gas, creating electron-ion pairs. The ionization electrons drift towards the anodes at the end of the TPC, whereas the positive ions drift toward the cathode in the middle of the chamber. In figure 6 at page 13, the TPC construction is shown.

A gas amplification system provides strong electric fields, which accelerates the incoming electrons. From that acceleration, the electrons gain energy and can ionize the gas molecules further. In this way an avalanche of electrons is created and the signal is amplified. The location of the avalanche can be measured by segmenting the anode plane into small areas, called pads[7]. Depending on the kind of avalanche chamber used, the moving charges either induce signals on the pads or are directly collected on the pads.

Three dimensional coordinates are obtained from the known coordinates of the pads and by measuring the drift time of the electrons. When the drift velocity of the electrons in the gas is known, the drift length can be calculated from the drift time and consequently a z-coordinate is obtained. From a large number of measured points on a trajectory, the track of the traversing particle can be reconstructed. In the ILC TPC, up to 400 measured coordinates along the track are needed to obtain the desired momentum resolution.

The TPC is embedded in a uniform, strong magnetic field, parallel to the electric field. The

presence of a magnetic field allows measurements of the particle momenta since the charged particle will bend off in a curved trajectory defined by its momentum. The TPC can also provide particle identification by measuring the ionization energy loss, $\frac{dE}{dx}$, of the electron [13].

The magnetic field improves the space point resolution since it decreases the effect of the transverse diffusion of the electrons during their drift towards the pads[7]. It is the diffusion of the drifting electrons that defines the position resolution.

TPCs have been used in many collider experiments and have performed very well. But until now, the TPCs were read out by wire technique, MWPC (Multi Wire Proportional Chambers). A new technique with a Gas Electron Multiplier (GEM) read out system developed in 1996 provides potentially superior position resolution, and hence a correspondingly better momentum and an improved two track separation. This system is planned for the ILC TPC if the prototype tests verify that the design goals can be reached.

3.1 Primary Ionization

When the charged particle enters the gas volume, it interacts electromagnetically with the gas molecules and primary electrons are liberated leaving a positively charged ion behind. If the energy of the primary electron is larger than the ionization energy (the energy required to ionize the gas atom), the primary electron can ionize the gas further to create a secondary electron-ion pair, these electrons are called delta electrons. This is unwanted, as the range of the delta electron can be several millimeters, which deteriorates the position information. But the phenomenon is unavoidable and results in a Landau shaped $\frac{dE}{dx}$ distribution.

The number of primary ionization electrons for most gases is proportional to the average atomic number, Z, of the gas atoms[7], and the spatial resolution increases with increasing number of electrons. The total number of ionization electrons can be expressed as

$$N_{eff} = \frac{E-I}{W} + 1$$

where E is the energy deposited by the incoming particle, i.e. the energy loss, I is the ionization potential and W is the effective energy required to create an electron-ion pair. Ionization does not require an exact amount of energy, but a threshold energy is required.

3.2 The gas

The gas used in the TPC prototype is a mixture of 95% argon, 3% CF4 and 2% isobutane. This gas has a fast and stable drift velocity at a low electric field, which simplifies the design of the chamber[13].

Different gases have different drift velocities. Higher drift velocity makes the drifting electrons suffer less from diffraction and thereby reduces the diffusion. The gases with high drift velocity, on the other hand, give worse resolution in the time dimension, since it takes shorter time to reach the read out pads.

If the gain of the avalanche chamber is set too high, the excessive liberated charge distorts the electric field and the proportionality is lost in the amplification. With too high voltage, a discharge in the gas can occur in the avalanche chambers. A discharge is a chain reaction of many avalanches. To avoid a discharge in the gas, a quencher must be present to absorb the photons emitted from the avalanche. The photons have high probability to ionize atoms in metallic surfaces. Such photo ionization electrons start new avalanches and so on. Traditional quenchers in

TPC gases are hydrocarbons which absorb photons and de-excites without electron emission, but the hydrogen in such gas mixtures has a large cross section for interacting with low energy background neutrons which will be crossing the TPC at ILC[14]. The quencher must therefore have a low concentration of hydrogen to minimize the background hits with large energy deposit, due to neutron-proton scattering. It is also important to reduce the oxygen and water in the chamber since it captures the drifting electrons.

3.3 Detector effects

The measurement is affected by various effects which are related to the detector, such as variations of the gas pressure and temperature, as well as inhomogeneities in the magnetic and electric fields. To minimize or avoid negative detector effects and optimize the reconstruction of a particle trajectory, simulations and prototype studies of the TPC are necessary.

3.3.1 Diffusion

Diffusion is a phenomenon that arises when the electrons scatter on the atoms in the gas. In the absence of an electric field, the electrons and ions diffuse uniformly outward from their point of creation. When an electric field is applied, the electrons and ions accelerate along the field lines towards the anode resp. the cathode, but there is still a diffusion phenomenon which makes the charge cloud smear out. This *smearing out* of the charge cloud makes the charge hit several pad segments, and a determination of the cloud centroid is possible. Thus, the track position can be calculated with an accuracy that is significantly smaller than the pad size. However, if the diffusion of the drifting electrons is too large, it will also contribute to decreased space point resolution. To determine the optimal spread of the cloud on the pads is an important part of the TPC test plans.

When the drift distance from the ionization point to the readout system is long, diffusion becomes a problem and the spatial resolution will be affected. With a magnetic field parallel to the electric field, the electron displacement due to diffusion is reduced since the magnetic field confines the electrons to trajectories along the drift direction and hence the transverse diffusion (perpendicular to the field) decreases. The longitudinal diffusion is unaffected, but this does not affect the two dimensional spatial resolution, as the transverse diffusion does. A magnetic field can reduce the diffusion by a factor 10 [6].

In figure 3, the diffusion constant and the drift velocity in the gas mixture used in the prototype as functions of the drift field is plotted. As can be seen from the figure, the transverse diffusion is $\sim 100\mu m/\sqrt{cm}$ at 1T for a drift field of between 100-250 V/cm, which coincides with the minimum diffusion and the maximum drift velocity as given by the curve marked W in the plot. The electric field used in the test experiment was 230 V/cm. The diffusion and drift velocity can be expressed in terms of the electron mobility. For optimal performance, the electron drift velocity should be relatively large, and the transverse diffusion constant relatively small in presence of the strong magnetic field [10]. The final ILC TPC will operate under a strong magnetic field of 4 T which gives a small diffusion constant (see figure 3).

For the GEM readout system, it is beneficial to have its large transverse diffusion in the amplification region to ensure that the charge is smeared out over more than one pad.

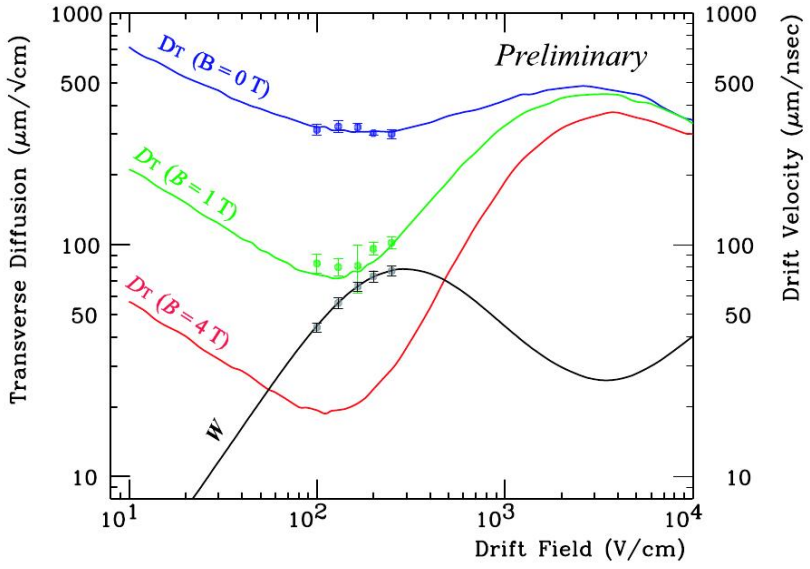

Figure 3: Simulation and data points of the transverse diffusion in the gas used in the prototype TPC for different strength of the electric and magnetic fields. The black line describes the drift velocity of the gas and has its maximum at 250 V/cm.[1]

3.3.2 E × B effects

In a MWPC, the electric field is not parallel to the magnetic field close to the wires. Thus, the combined effect of the two fields, **E** × **B**, will have a transverse component, which causes a degraded space point resolution. This effect is reduced in a TPC with GEM readout system. To avoid the drifting electrons to deviate from straight trajectories, i.e. in order to minimize the diffusion of the electrons, the **B** and **E** field must be perfectly aligned (parallel) and uniform. This can only be achieved to some finite precision and a calibration system based on lasers liberating electrons at known coordinates must be used to provide the absolute coordinate system.

3.4 Gas Electron Multiplier (GEM) and read out pads

To obtain good position resolution - that in the end leads to good momentum and mass resolution - the diffusion must be low and the pad size must be accordingly small in order to allow sharing of charge on several pads so that the centroid of the cloud can be determined. GEM TPCs allow a different pad geometry with a pad width of $\sim 1mm$ and hence a smaller anode-pad distance can be obtained which is preferable for the position resolution (and necessary at very high magnetic fields).

GEM is a new read out system for the TPC and consists of a 50 μm [8] kapton foil with copper layers on each side and a large number of 50μm diameter holes separated by 100-200 μm, see figure 4(b). High voltage is applied between the copper layers and the voltage difference creates a large electric field within the GEM holes (40-80 kV/cm), see figure 4(a). When the drifting electrons enter the high field region in the holes, they ionizes the gas in a cascade and an avalanche occurs.

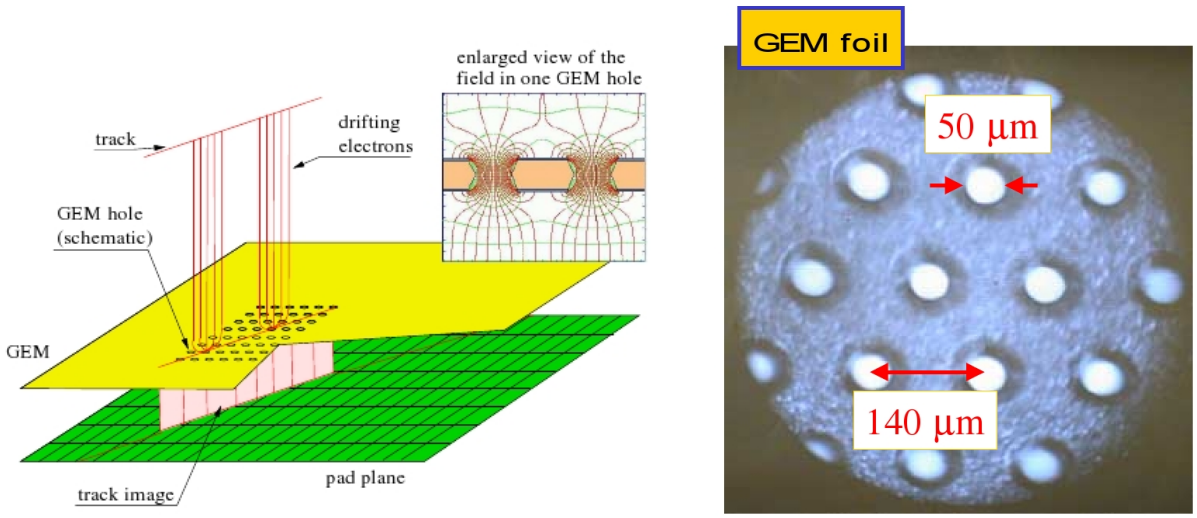

(a) A schematic view of the GEM technique.

(b) The GEM holes in the kapton foil.

Figure 4: The GEM read out system. (a) from ref. 8 and (b) from ref. 5.

The amplification can be 10^3 for a single GEM. The charge is collected on the read out pads located a few mm behind the GEMs, see figure 4(a), and a projected image of the track can be obtained. With only one GEM foil, the amplification is likely to be insufficient [8]. To solve this, several GEM foils can be used.

3.4.1 Positive ion build up

Due to the creation of electron-ion pairs from the ionizing charged particles and the build up of an avalanche in the GEM system, there will be a positive ion accumulation in the drift volume and on the surface of the gas amplification plane due to the fact that the positive ions will slowly drift back to the central cathode. If the amount of positive charge is too large, the electric field properties of the TPC may become distorted. Eventually, this could influence the rate capability of the detector, thus limiting the physics sensitivity of the experiment. The problem is though larger in a wire chamber than in a GEM TPC since the positive ions produced in the avalanche process are swept onto the metal foils of the GEM and do not reach the drift region[8]. The back drifting ions can be minimized by using low gas gain and gating, such that only triggered events are allowed to develop avalanche multiplication [14].

3.5 Background

In the final TPC, there will be ionizing background radiation from the accelerator, from cosmic rays and other sources. Out of these the main source of background comes from beam-strahlung processes, which is due to the fact that the bunches affect each other mutually when they cross such that the electrons and positrons will change directions in the electric fields generated by the bunches and emit synchrotron radiation. These photons may either enter the detector itself or hit

the material in the accelerator and create hadrons out of which the neutrons constitute the most severe background [14].

3.6 Advantages with a TPC

The goal for the final ILC TPC is 400 precise measurements along a track with a track reconstruction efficiency of 99% [11]. The spatial resolution of the final ILC TPC needs to be down to be 100 μm with a magnetic field of 4 T, see figure 5(a). This goal requires new technology such as the GEM readout system since a wire chamber cannot reach these levels and is therefore not an option [1]. The reason for the limited resolution with wire chamber readout is that wire chambers have a different position response along and across the wires and the actual signal, the image charge has large extensions.

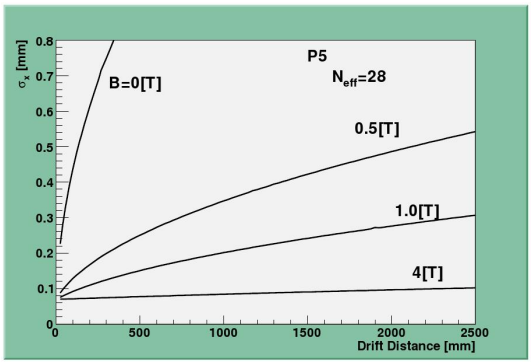

(a) Spatial resolution for a GEM TPC. (ref. 11)

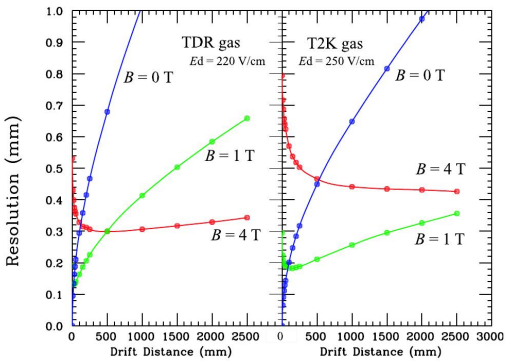

(b) Spatial resolution for a multi wire TPC in different gases. (ref. 1)

Figure 5: Simulated space point resolution as a function of the drift distance for different magnetic fields and gases.

Measurements at drift distances between 70-200 mm will be analyzed in this report, which means that the variation in resolution is only expected to vary 100-200 μm, see figure 5(a). The TPC prototype operates in 1 T, while the ILC TPC will operate at 4 T, giving a space point resolution of ~ 100 μm.

The GEM read out system has a clear advantage over multi wire TPCs concerning the spatial resolution. A simulation of the spatial resolution in a multi wire TPC for different drift lengths and different magnetic fields can be seen in figure 5(b). Compared to the simulations in figure 5(a), the spatial resolution is clearly better for GEM TPCs. Other advantages over wire read out are improved two particle separation (space point resolution dependent), the signals are distributed over a smaller area, few positive ions in the drift volume and the $\mathbf{E} \times \mathbf{B}$ effect is reduced.

3.7 Momentum resolution

The trajectory of a track is measured by measuring the coordinates in space. From that, the radius can be determined and the curvature and hence the momentum can be calculated. For the transverse momentum, the resolution in the x-y-plane is required, but when the invariant mass resolution for new created particles is wanted, the total momentum vector for the particles must be known with a good accuracy.

The transverse momentum resolution is described by

$$\frac{\sigma_{p_T}}{p_T} \propto \frac{p_T \sigma_{spatial}}{L^2 B}$$

where p_T is the transverse momentum, $\sigma_{spatial}$ is the spatial resolution, B the magnetic field and L the track length (the length is proportional to the number of samples) [4]. The track length is crucial here; the resolution improves with increasing track length. The momentum resolution goal for the ILC experiment is $5 \cdot 10^{-5} GeV^{-1}$ [10].

One important goal of the prototype test is to optimize and measure the position resolution so that the momentum resolution of the final TPC can be verified.

4 The experiment at DESY

4.1 The experimental setup and the readout electronics

Figure 6(a) gives a schematic view of the TPC prototype set-up with the magnet and the trigger scintillators for cosmic muons. The coincidence signals of the two scintillators trigger the readout system. Figure 6(b) shows the TPC prototype field cage half way in the superconducting solenoid magnet.

4.1.1 The pad modules

In figure 6(c), the pad planes, or the *modules* are seen as seven panels at the electronics end of the TPC. In this experiment, one and three modules are used, marked as red in figure 6(c). The modules are equipped with pads at one side, see figure 7(a), and connectors at the other side, figure 7(b). The flat kapton cables are connected to the connectors at the modules.

The pad front of the module is turned towards the inside of the TPC. The modules are divided in two sections: the lower section has 176×14 pads and the upper has 192×14 pads, thus the pad width increases with increasing layer number, see figure 7(a) and 8. This means that the pads on the pad area of the module is complicated to map in the tracking software.

The pad layers (figure 7(a) for definition) are orientated vertically in the beam test, i.e. perpendicular to the beam, and horizontally in the cosmic ray mode, in order to have the tracks along the longer pad dimension, as will be the case for high momentum tracks in the final TPC. This minimizes the influence of angular effects on the spatial resolution since the short side of the pads will be perpendicular to the track and hence the position resolution can be evaluated more accurately.

The pad modules of the prototype back plane are built in the shape of the final modules as they will be mounted in a full size TPC at a radial distance of 1.332 m from the beam axis to the center module at the prototype TPC, see figure 9.

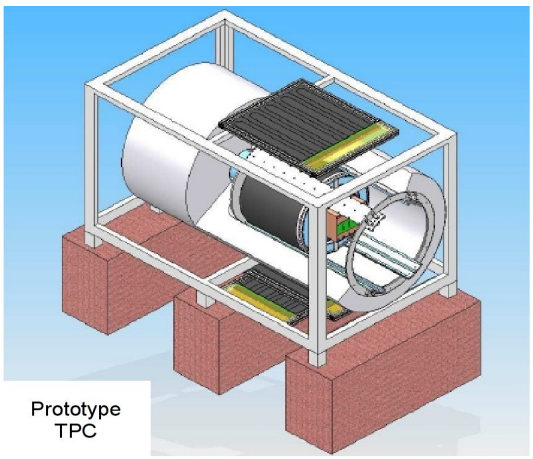

(a) Schematic view with a cut through the magnet of the experimental setup at DESY.

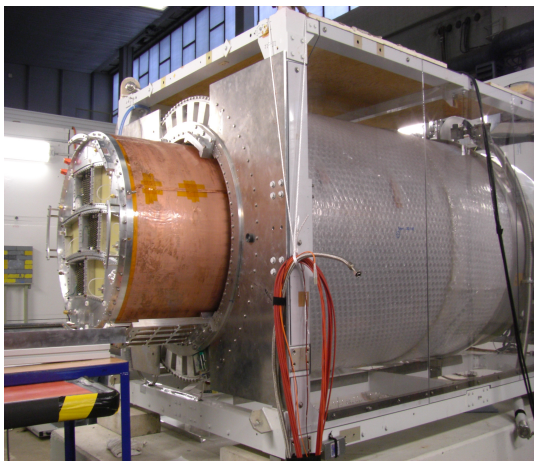

(b) The TPC field cage prototype at DESY half way into the magnet.

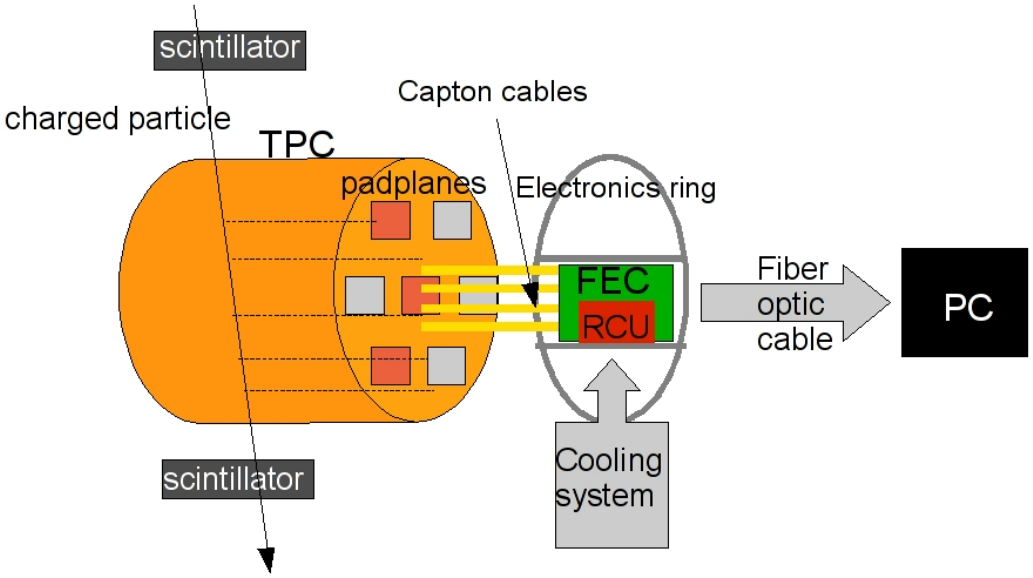

(c) The experimental setup. The different components are explained in the text.

Figure 6: The prototype TPC at DESY.

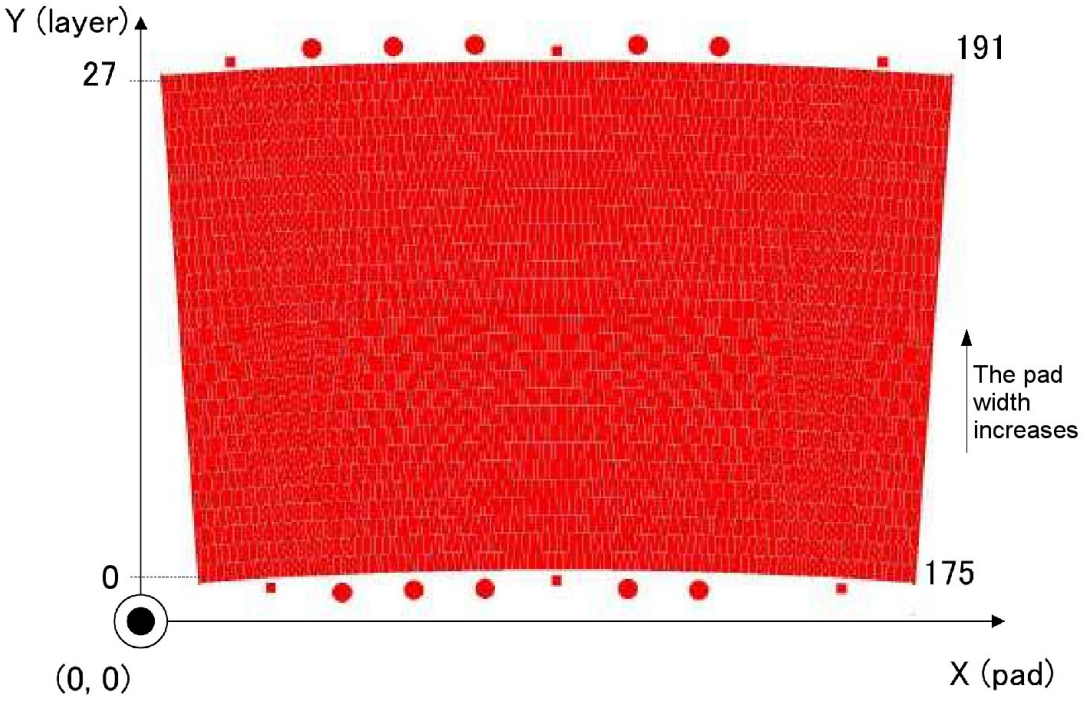

(a) The pad geometry viewed from inside the TPC.

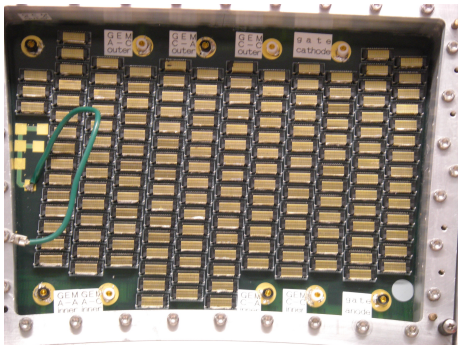

(b) A pad plane with connectors, viewed from outside the TPC.

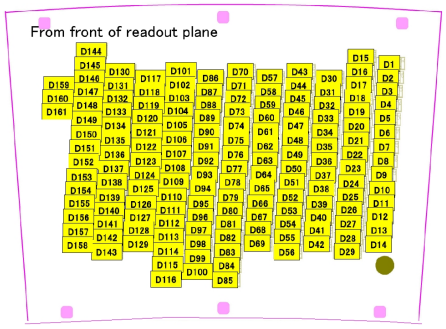

(c) A schematic view of the pad plane with connector numbering.

Figure 7: The pad and connector geometry viewed from inside resp. outside the TPC.

layer #	# of pads	pitch (width, gap)	staggered half of pitch	pad height (gap = 0.1)
27	192	1.20 (1.10, 0.10)	->	5.26
26	192	1.20 (1.10, 0.10)		5.26
25	192	1.19 (1.09, 0.10)	->	5.26
24	192	1.19 (1.09, 0.10)		5.26
23	192	1.19 (1.09, 0.10)	->	5.26
22	192	1.18 (1.08, 0.10)		5.26
21	192	1.18 (1.08, 0.10)	->	5.26
20	192	1.17 (1.07, 0.10)		5.26
19	192	1.17 (1.07, 0.10)	->	5.26
18	192	1.17 (1.07, 0.10)		5.26
17	192	1.16 (1.06, 0.10)	->	5.26
16	192	1.16 (1.06, 0.10)		5.26
15	192	1.15 (1.05, 0.10)	->	5.26
14	192	1.15 (1.05, 0.10)		5.26
13	176	1.25 (1.15, 0.10)	->	5.26
12	176	1.24 (1.14, 0.10)		5.26
11	176	1.24 (1.14, 0.10)	->	5.26
10	176	1.23 (1.13, 0.10)		5.26
9	176	1.23 (1.13, 0.10)	->	5.26
8	176	1.22 (1.12, 0.10)		5.26
7	176	1.22 (1.12, 0.10)	->	5.26
6	176	1.21 (1.11, 0.10)		5.26
5	176	1.21 (1.11, 0.10)	->	5.26
4	176	1.20 (1.10, 0.10)		5.26
3	176	1.20 (1.10, 0.10)	->	5.26
2	176	1.20 (1.10, 0.10)		5.26
1	176	1.19 (1.09, 0.10)	->	5.26
0	176	1.19 (1.09, 0.10)		5.26

Figure 8: Pad geometry: the modules are divided in two sections of 14 pad rows, or *layers* each. The lower section has a width of 176 pads and the upper part as a width of 192 pads. section has. The pad width increases with the layer number, but the height is constant.

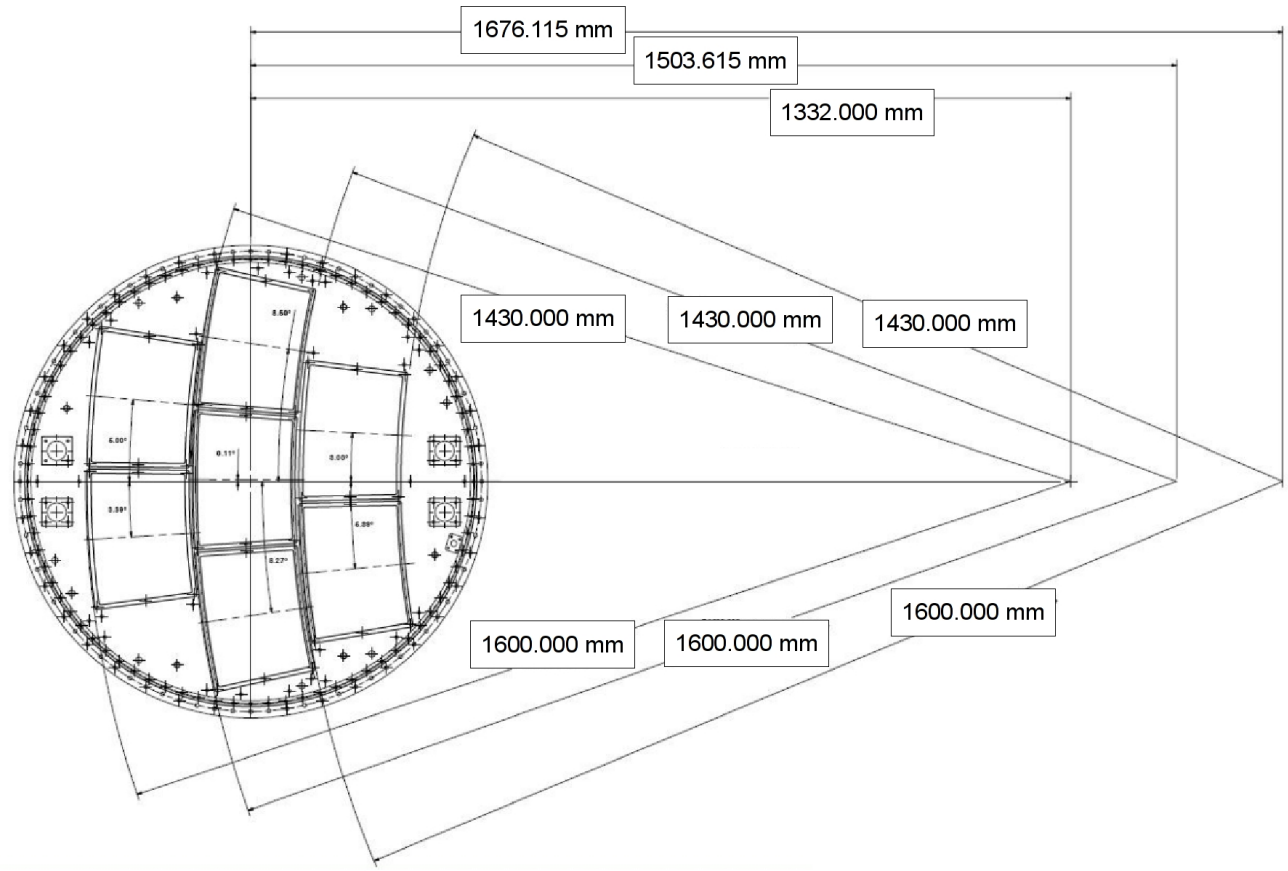

Figure 9: The prototype TPC module plane is a part of the final TPC module plane.

4.1.2 The electronic readout system

32 pads (two rows with 16 pads each) are connected to one connector. The cables connect the pads to the FEC (Front End Card) that serves four cables (128 pads), see figure 11(a) and 11(b). To hold the kapton cables in place and in order to shield the FECs from external noise, the cables are pulled through narrow slits in a shield which is positioned in the electronics crate in front of the FECs, see figure 10(b) and 10(c). The FEC serves 64 channels on each side. In this first step of the experiment, we use 24 FECs when operating one pad panel, and 26 FECs when operating with three panels in beam mode, see figure 18 and 19. The charge deposited on the pads are read out in the following way:

- A charge sensitive preamplifier in which the charge induced on each pad is converted to a voltage, proportional to the charge.
- A shaping amplifier: the voltage pulse is amplified and shaped in time with the Gaussian pulse shaper. The preamplifier/shaper chip, PCA16, has been developed for this project. It contains 16 channels of the preamp-shaper function.
- The ALTRO (ALice Tpc ReadOut) chip, which is an integrated circuit, contains 16 channels. There are 8 ALTROs on one FEC - giving 128 channels per FEC. It performs pedestal subtraction, zero- suppression, formatting and buffering.
- The data must be in digital form so that a computer can handle it. An analog to digital converter (ADC) in the ALTRO chip converts the analog signal to a corresponding digital value with a sampling frequency of 20MHz, which covers the full drift time with at most 1000 samples.
- The FECs, which are read out via a 32 bit wide data bus controlled by one RCU (Readout Control Unit) that transfers the digital data for each time bin and each pad via an optical fiber to the DAQ computers.
- The data from an event in the TPC is for each pad composed of 1000, 10 bit ADC values which are proportional to the collected charge on the pad. The samples are taken every 50ns (20MHz) and each sample corresponds to a certain drift time after the system was triggered by the passing particle.

A pulse is seen as a peak above the pedestal where the charge contained in the pulse is defined by the amplitude of the pulse. Data are recorded on-line with a software that allows us to check the charge in terms of ADC channels for each of the 1000 time slots (samples) for every pad. Special pedestal runs are performed with no in-signal in order to control and analyze the noise fluctuations of the baseline. The noise is problematic when it has a periodic shape. Except from a few problematic noisy channels, the average noise is very low, see noise analysis in reference 3.

4.1.3 Control parameters

The settings of the amplifier chip, PCA16, can be programmed by a bit sequence sent to the front end card. The programmable parameters are the shaping time, the gain and the decay time. The shaping time is the time during which analog information is filtered out. The shaping time should

(a) Kapton cables connected to the pad connectors.

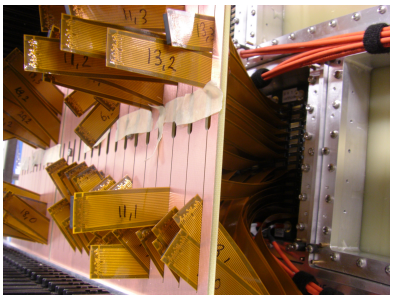

(b) Kapton cables from the pad connectors through the slits.

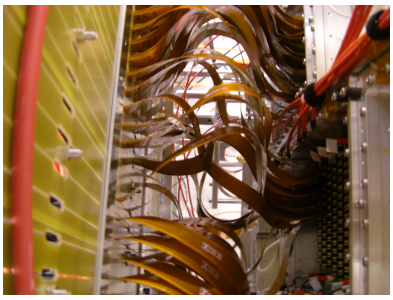

(c) Kapton cables in three pad planes.

Figure 10: Kapton cable connection. The high voltage cables (red) are also visible.

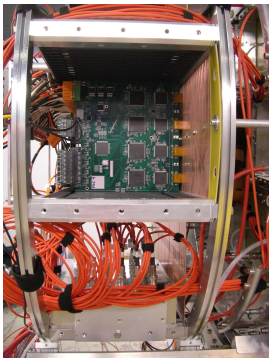

(a) FEC in the electronics ring.

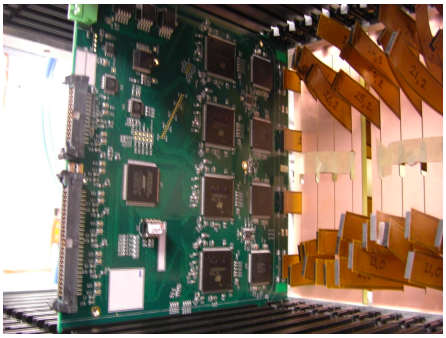

(b) One FEC connected.

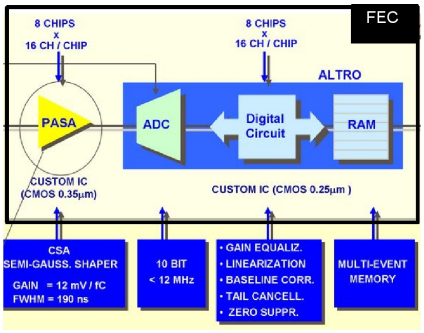

(c) FEC block scheme.

Figure 11: FEC located in the electronics ring connected to the kapton cables.

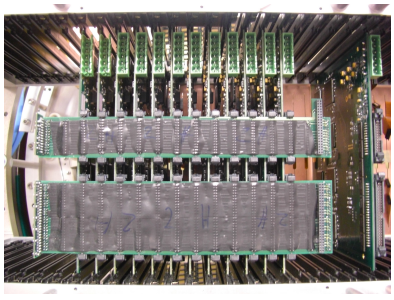

(a) The FEC:s are read out by a 32 bit data bus.

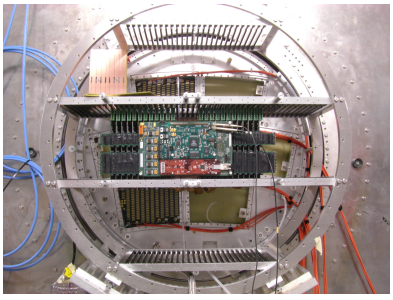

(b) The electronics mounting ring with FECs and the RCU.

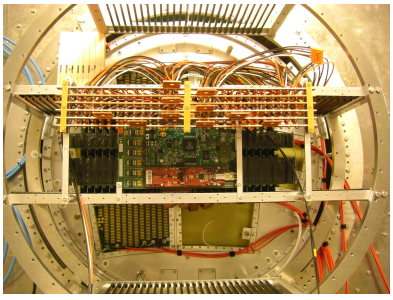

(c) The low voltage rails distribute LV to the readout electronics.

Figure 12: The FECs readout system.

be matched to the time characteristics of the incoming charge cloud. Different shaping time gives different rise time of the output pulses. The rise time is the time difference from which the pulse appears to the time at which it reaches its maximum (peak time). The shortest shaping time corresponds to 30 ns rise time and the longest to 130 ns rise time, the latter of which has been mostly used during the measurements reported here. The gain can be varied in four steps between 12 mV/fC (gain 0) and 27 mV/fC (gain 3).

4.1.4 Zero suppression and pedestals

With zero suppression, data that does not fulfill the requirements for the definition of a pulse is deleted. The definition of a pulse is three consecutive samples with ADC values above a given threshold. A well set threshold should allow zero samples to be above threshold in at least 10% of the cases. The conclusion of this is that before taking too much data with zero suppression, the ADC threshold has to be adjusted to be consistent with this requirement. The fact that it is the first test with a new system, data without zero suppression is important for the following reasons:

- The hardware zero suppression is designed for the ALICE application and it has to be evaluated for the prototype TPC pulses.
- There has been problems with the data read out in zero suppression mode and data discarded due to zerosuppression cannot be retrieved afterwords.
- The zero suppression must be evaluated quantitatively before zero suppression can be fully implemented.

4.2 Cooling system

The temperature in the space between the FECs must not be too high. Ideally it must be below 50 degrees, since the components can be destroyed due to overheating and unstable operating temperature can also cause drift in the baseline level. We measured the temperature between the FECs without a cooling system and obtain the following results:

- When the FECs were oriented vertically so that the air could flow between them by convection, the temperature was stable around 30 degrees Celsius.
- When the FECs were rotated horizontally, the temperature rose to 60 degrees and still increasing. For this reason it was necessary to install a fan system, see figure 13.

The fan tubes, made of aluminum, must be long so that the fan motor can be placed outside the magnetic field, see figure 14. The TPC must also be able to rotate and pushed back and forth in the magnet.

When the TPC was rotated (90 degrees), such that the FECs were horizontally directed and the fans were on, the temperature was 20 degrees at the hottest spot.

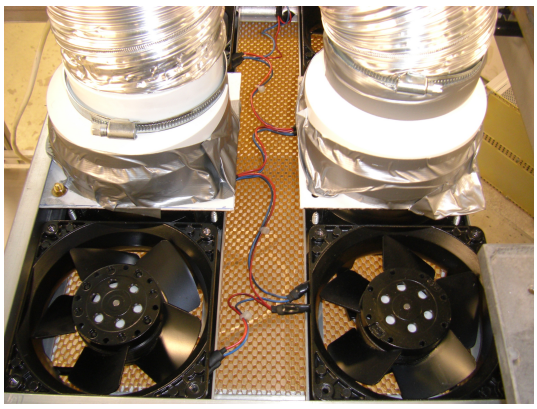

(a) Four fans located on a horizontal table were used. The tubes are made of aluminum on a plastic base.

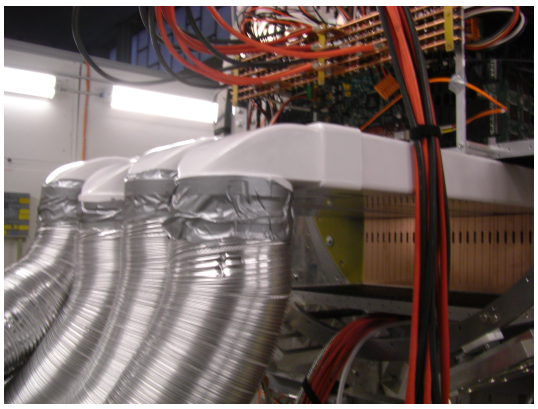

(b) The transport of the air into the electronics ring, under the FECs.

Figure 13: The cooling system, based on forced air flow, allows operating the electronics, with the FECs oriented in any direction.

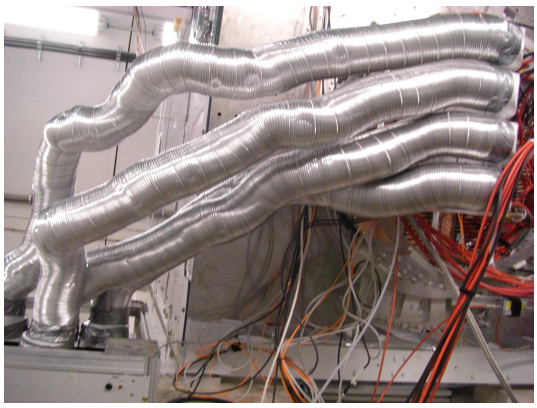

(a)

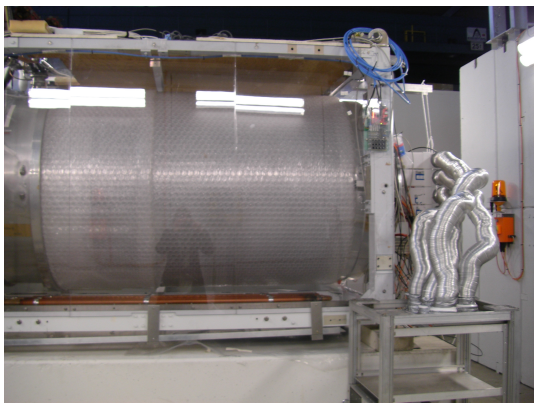

(b)

Figure 14: The tubes must be long enough to reach outside the magnetic field.

4.3 Cosmic ray data

The scintillators that generate a trigger signal are positioned above and below the field cage. The cosmics are mostly muons which comes in from all angles. This means that the cosmic tracks are three dimensional, compared to the beam tracks which are perpendicular to the TPC and thus only gives a two dimensional track. Muons that enters the TPC at different angles also induce more charge per pad since the projection of the track over a pad corresponds to a longer track length of the real track.

4.4 Electron beam data

The test beam used in the experiment is extracted from a bremsstrahlung beam which is generated by making the circulating beam of the electron and positron in the synchrotron DESY II hit a carbon fiber, see figure 15. The photons produced will then hit a metal foil and pair production (production of an electron-positron pair) takes place. The secondary beam will spread out with a dipole magnet and the final beam momentum and space definition is defined by a narrow collimator. Setting the magnet current chooses the beam momentum. [15]

The trigger scintillators, which define the traversal of particles in space and time, are positioned upstream in the beam line, between the TPC and the collimator hole, see figure 16.

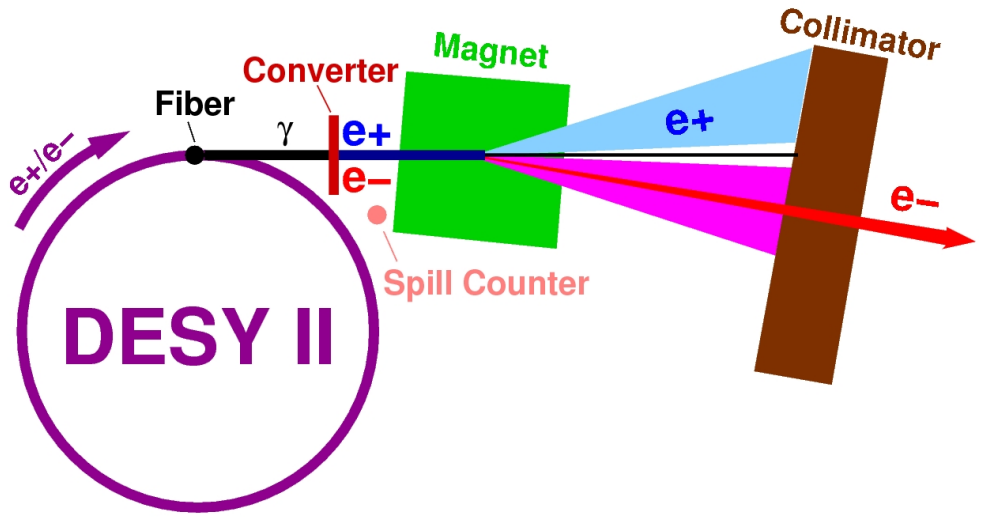

Figure 15: The test beam production.

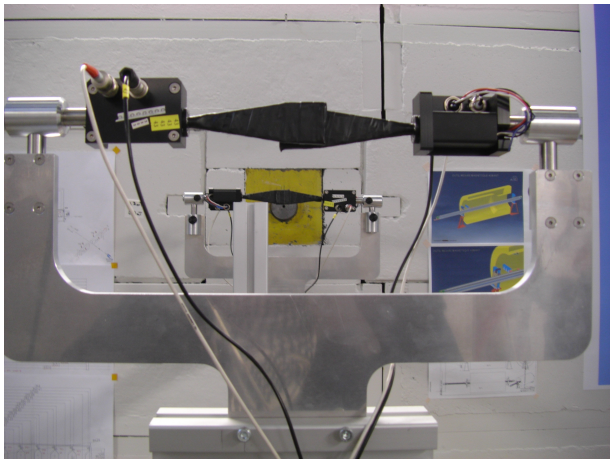

Figure 16: The scintillators are positioned upstream in the beam line, between the TPC and the beam hole to register when a beam particles enters the detector.

4.5 Active pad area

The collimated beam has a diameter of about 5 mm. Thus it was important to instrument a stripe of pads, sufficiently wide to fully contain the electron clouds from all possible track roads. The available electronics was thus sufficient to instrument three modules over the full TPC diameter. For cosmics on the other hand, the positions and directions of the triggering tracks vary a lot, so the central module was instrumented as much as possible for these measurements. Unfortunately, instrumenting one module was not a success since we then discovered that the lower half of the central module did not work. In beam mode, these pads were not instrumented, but instead these channels were used to reach longer in the beam direction and make the area somewhat broader downstream due to beam divergence.

It was important to organize the kapton cables connection to modules to minimize the vertical bending (in order to keep the noise low and prevent the cables to unconnect) and at the same time optimize them with respect to the area which was chosen to be instrumented. This is illustrated for the case of one module in figure 17, and in the case of three modules in figure 19. A logical system defining the channel number of the electronics with respect to the pad it is connected to was needed. Therefore a coordinate system code has to be developed in order to relate the channels of the FECs with the geometrical position of the pads. The mapping from a pin in the cable to a channel in a FEC is fixed. Thus, once a cable has been attached to a connector on the pad board, the full chain from pad (and its geometrical position) to channel number in the data is fixed.

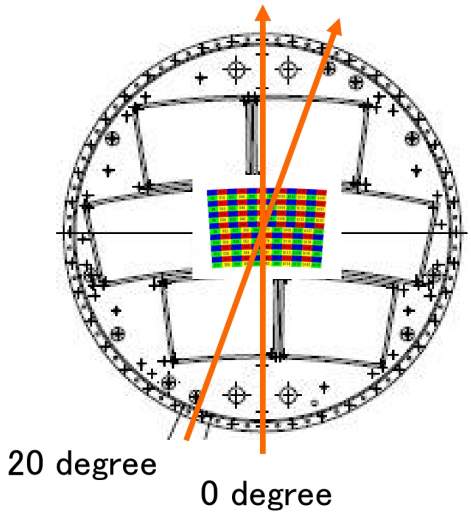

(a) The center module instrumented for tests.

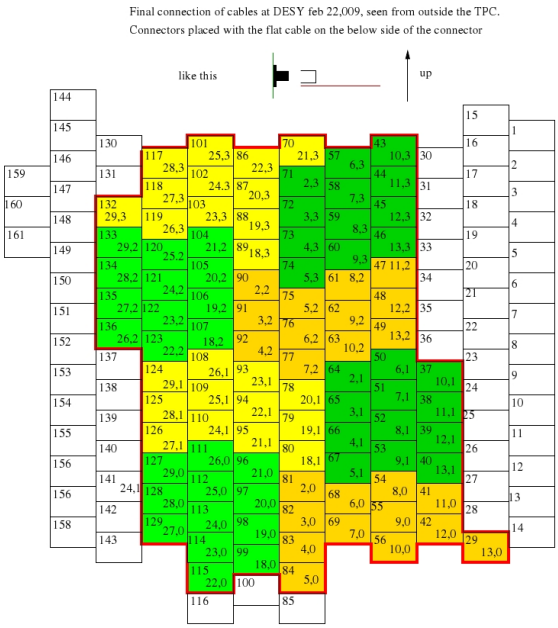

(b) The cable mapping for one module. One box represents one connector, the upper left number is the connector number, the lower right numbers is the FEC number and the cable number within the FEC.

Figure 17: The cable mapping for operating at one module.

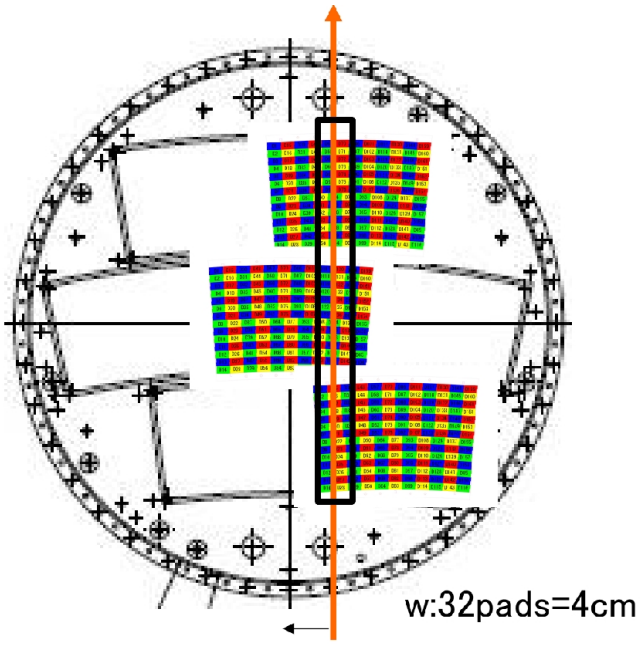

Figure 18: Beam mode: three modules are instrumented to get an elongated view for a track.

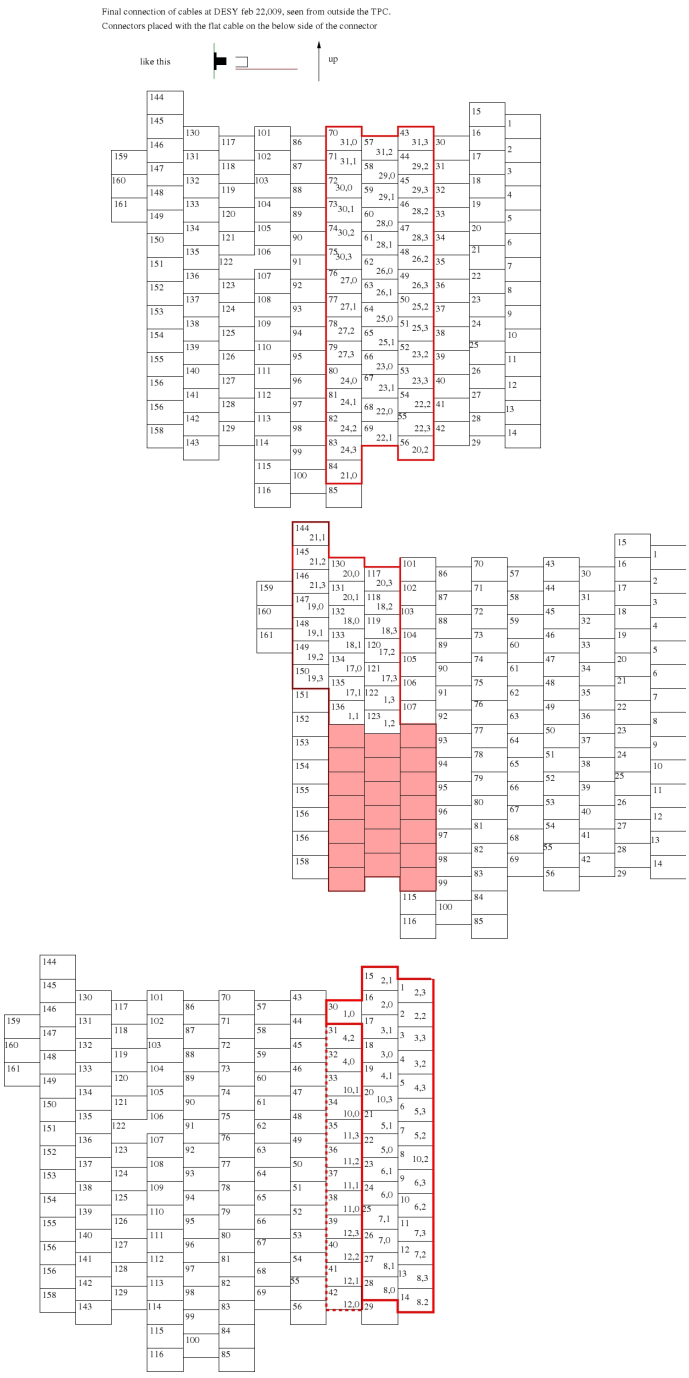

Figure 19: The mapping system for three modules in beam mode. One box is one connector, the upper left number is the connector number, the lower right numbers is the FEC number and the cable number. The lower half of the center module is not instrumented since it became clear using only this module that the GEMs on this half did not work.

5 Analysis and results

In the analysis of the test beam data from the prototype TPC at DESY, the focus is on track reconstruction and space point resolution. The position resolution is critical for the design of the ILC TPC readout geometry, as described in section 2. Reference 3 focus on time and noise studies.

A cluster finding algorithm for the tracking and position resolution analysis has been developed, and a somewhat simpler algorithm has been developed for a visualization of the tracks. The complex pad geometry and the fact that the GEM modules are separated and rotated with respect to each other makes the software construction difficult, in particular since all hardware was used for the first time. A special problem (which is still not fully solved) was how to position the different modules in a common coordinate system with a sufficient accuracy to match the anticipated resolution of the system. This problem is later described as the *systematic residual problem* since the distance of the cluster position to the fitted line (i.e. the residuals) which describes the track trajectory, has a systematic displacement. This problem is bypassed by analyzing single modules instead of all three modules together.

All the software is written in C++ within the ROOT analysis framework. C++ is an object oriented language and consists of pieces called classes and functions which can be created or loaded from the Standard Library. ROOT has routines for filling and displaying histograms, functions, graphs etc. It has well defined ways to handle an analyze within particle physics and in fact all physics where spectra are analyzed.

5.1 Track visualization

The first step in the analysis is to visualize the tracks event by event to study the geometry and the basic features of the recorded track trajectory. From this, ideas of how more advanced software should be constructed (such as clustering and tracking algorithms) can be obtained.

The pad geometry, as described in section 4.1.2, is complex with the pads having different amount of shift for each pad layer, the modules are separated, and the position coordinates for each module has an inaccurately known displacement. These are parameters that contribute to difficulties in making the reconstruction and visualization of the tracks general enough.

Anyway, to visualize the tracks in two dimensions (the data is averaged over time, i.e. the third dimension is not added), the space coordinates for pads corresponding to the electronic channels must be known. For this, a mapping table is created that relates a channel with its corresponding readout pad for which the space coordinates are known. With this raw mapping, the modules have an arbitrary position relative to each other. Alignment of modules in two dimensions is done by determining translation constants from the technical drawings. Possibly also rotations have to be implemented. The channel content (the charge in ADC value) is then read from a file containing a vector with the channel content for each channel. This file is extracted from a program that converts the binary data file to a file with the time bin data.

The channel content at the correct coordinates is then filled in a three dimensional histogram with the pad position in X and Y make up two dimensions in which the track position is shown in a simple way, while the charge is visualized with a color code in the third dimension or as a box height in a lego plot.

5.1.1 The results from the track visualization

The highest charge (in ADC channels) in each channel is plotted either as a color code, see figures 21-24 or as a lego box amplitude, see figure 20. The non operating lower half of the center GEM module is visible in these figures as the large hole interruption in the track. The other spacing is due to the dead area between the modules.

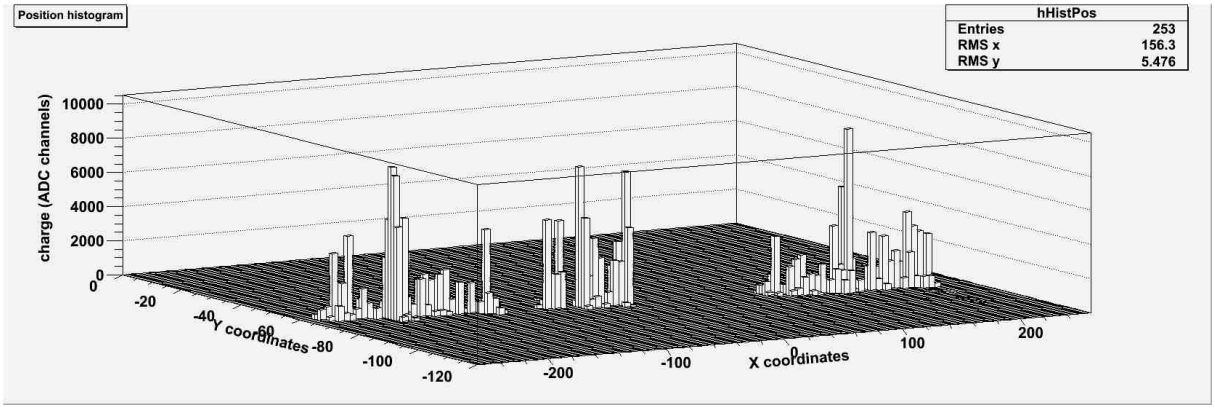

Figure 20: 5 GeV/c beam with magnetic field 1 Tesla, beam incoming from the right. The charge is in ADC channels and is shown as the amplitude of the lego boxes, proportional to the charge.

Without magnetic field, the track image is expected to be broader and the cluster width larger than with magnetic field on due to larger transverse diffusion. In figure 21 the track image in space coordinates for one single event without magnetic field is shown. Compared to figure 22, where the drift distance is the same as for the track in figure 21 (200 mm), and the only parameter varied is the magnetic field (1 Tesla), the track is indeed broader for the case with no magnetic field. The module spacing and the non working GEM can also be seen in the figures.

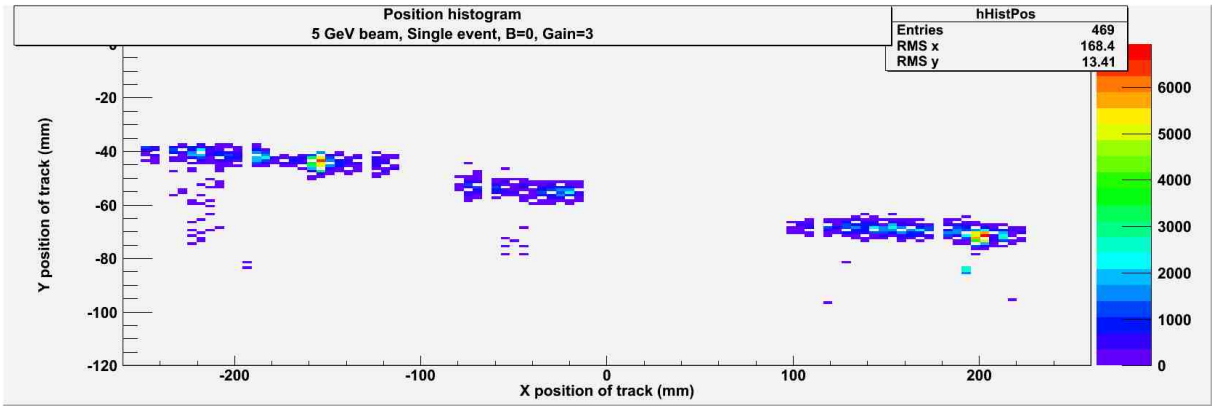

Figure 21: Pad image of a track from a 5 GeV/c beam, without magnetic field, drift distance 200 mm, one single event.

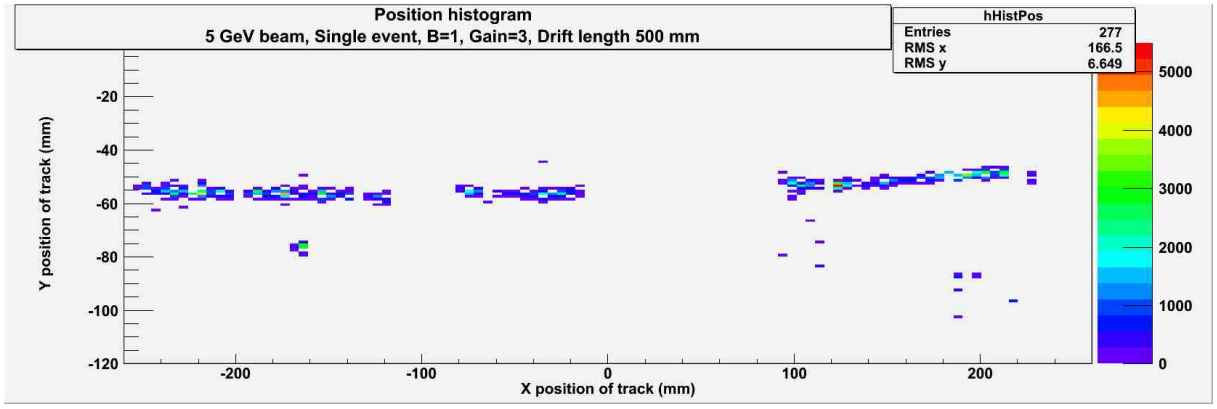

Figure 22: Pad image of a track from a 5 GeV/c beam, with magnetic field 1 Tesla, single event, drift distance 200 mm.

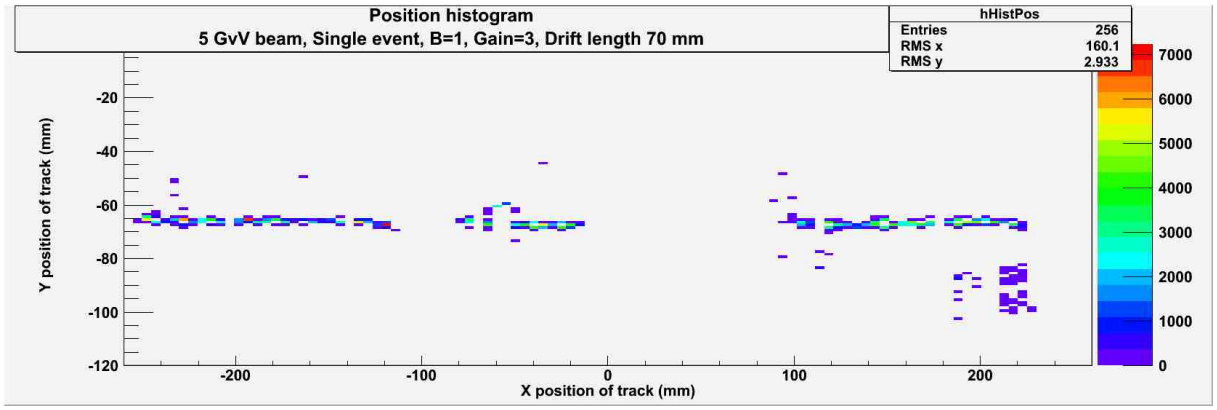

Figure 23: Track image from a 5 GeV/c beam, magnetic field 1 Tesla, drift length 70 mm.

The narrower a track image is, the better position resolution in the bend plane can be obtained. The position resolution is expected to be better with decreasing drift distance, and it is therefore interesting to visualize tracks where the ionization electrons have traveled different distances. Figure 22 and 23 shows the track image for one varying parameter, namely the drift distance. Comparing the width of the track for the different cases shows that the shorter drift length (70 mm) gives a narrower image and a smaller cluster width than drift distances of 200 mm, as expected from simulations about the diffusion, see figure 23.

The main goal with the track visualization is now completed by comparing tracks with magnetic field on and off, and tracks with different drift length. The results show that the track width, and hence the cluster width, is behaving like expected. The geometrical mapping constant also appears to be under control since tracks are reasonably well reconstructed. But other interesting observations can be done from the track visualization:

Firstly, noisy pads are seen at a concentrated area which corresponds to specific channels. Using non-zerosuppressed pedestal data, the noise fluctuations of the baseline, i.e. how the ADC channel differs from the average level representing zero input charge, can be measured. Noise can be either random noise due to the inherent noise in the amplifier channel or pickup noise from e.g. antenna pickup from the environment in the unshielded kapton cables and grounding problems. The pickup noise has normally some sort of time dependence. If there is a time structure of the noise, it must be investigated further and reduced if possible. Except from some systematic noise areas seen in the track visualization plots, figure 21 - 23, the data are very clean, i.e. the noise is low. To reduce the noisy area, a time window is set in the clustering and tracking software, which selects the time where tracks can appear. For more analysis results on the noise, see reference 3.

Secondly, the track visualization plots with magnetic field 1 Tesla (figure 22 and 23) shows module edge distortions of the track image. This must be further analyzed. The preliminary explanation is that this is due to distortions of the electric field at the module edges causing non-parallel **E** and **B** fields.

And thirdly, the analysis of the track images shows a small fraction of events where delta electrons are visible, i.e. electrons that ionizes more, or events with multiple tracks, see figure 24. I will not analyze these events further.

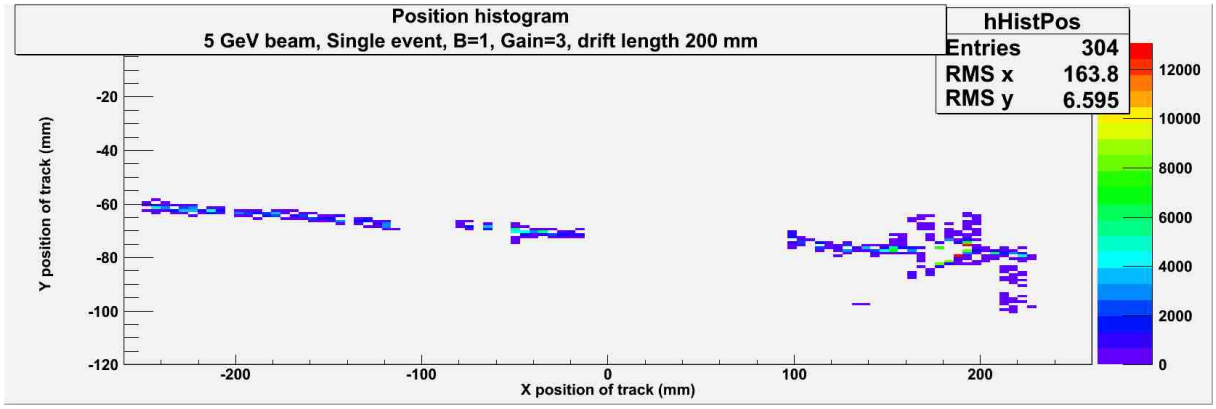

Figure 24: Delta electrons.

5.2 Cluster finding

Cluster finding provides the first step in the reconstruction of tracks in a more advanced and accurate way than in the visualization. The idea is to group signals, pad layer by pad layer, belonging to the same track and calculate the hit position. Figure 25 is a block scheme of the cluster finding algorithm.

The clustering is done on data which is time averaged, i.e. it is the projection of the track on a two dimensional plane that is used for clustering, and not three dimensional with the time setting the third coordinate. This is not a permanent way of clustering and tracking, since it only allows one track per event - which is not the case for the final ILC TPC where an event will contain several tracks.

5.2.1 Analysis software - Cluster finding algorithm

The cluster finding algorithm is constructed as follows (a block scheme can be seen in figure 25). First, the binary data file is converted to a root-file and a Tree is created where all the data is stored, e.g. the charge for each channel. In the second step, the program reads in the mapping, i.e. the module number, layer number and pad number for each channel. The channel number for each pad-layer coordinate is then stored in a matrix, see the block scheme (figure 25). A time window is set to reduce noise that comes in to the system at a different time. This is done by reading off the time interval for the pulse peak of the signal.

A histogram with the charge for each channel in the correct pad-layer coordinates is filled, and thus gives an image of the track similar to the track visualization image. This is the raw mapping, i.e. it is correct in the track (layer) direction (see figure 26) , but displaced in the other direction due to the non aligned modules. This is not a problem though, since the clustering will be done in the track direction in the pad-layer coordinate system and then translated to the space coordinate system with a displacement constant added.

The program loops over every x and y bin (cluster finding in the direction perpendicular to the track) and finds the charge value in the current x bin - y bin position. If the charge value is less than, or equal to, the value for the previous and next x-bin, the procedure continues. The maximum charge in one layer defines the peak, and the cluster is found around this peak.

The clustering part is now done and the centroid of the cluster must be calculated in order to do the tracking part. The weighted mean of the cluster position is calculated by:

$$< x >= \frac{\sum q_i x_i}{\sum q_i}$$

where q_i is the collected pad charge and x_i is the bin-position (the x direction is seen in figure 26, i.e. perpendicular to the track). The cluster positions in the raw pad-layer histogram can be seen in figure 27.

The cluster centroid position is then translated into x and y coordinates in space (mm), see figure 28. The Tree is filled with cluster information such as module, layer, total charge, maximum charge in one pad-time bin, cluster width and space coordinates. Figures 30, 31 and 32 shows the cluster position in x and y space coordinates. These are the reconstructed cluster coordinates on which analysis such as position resolution and momentum determination can be done.

To reconstruct tracks, a second degree polynomial function is fitted to the cluster position coordinates. A fit is also made to the single modules, to be able to analyze them one by one since the module edge deviations were discovered in the track visualization analysis. The distance

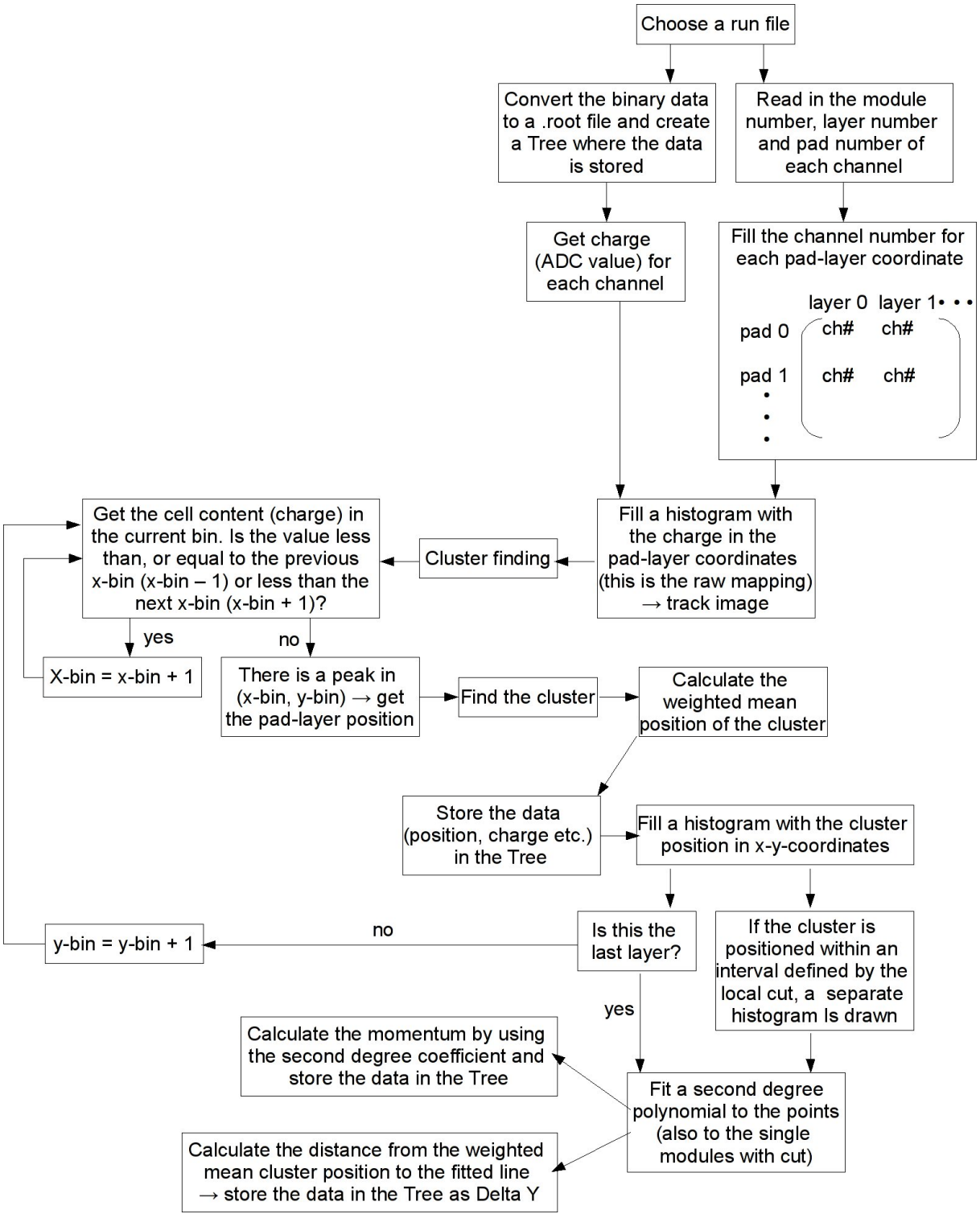

Figure 25: A block scheme of the Tree construction algorithm, involving the cluster finding part.

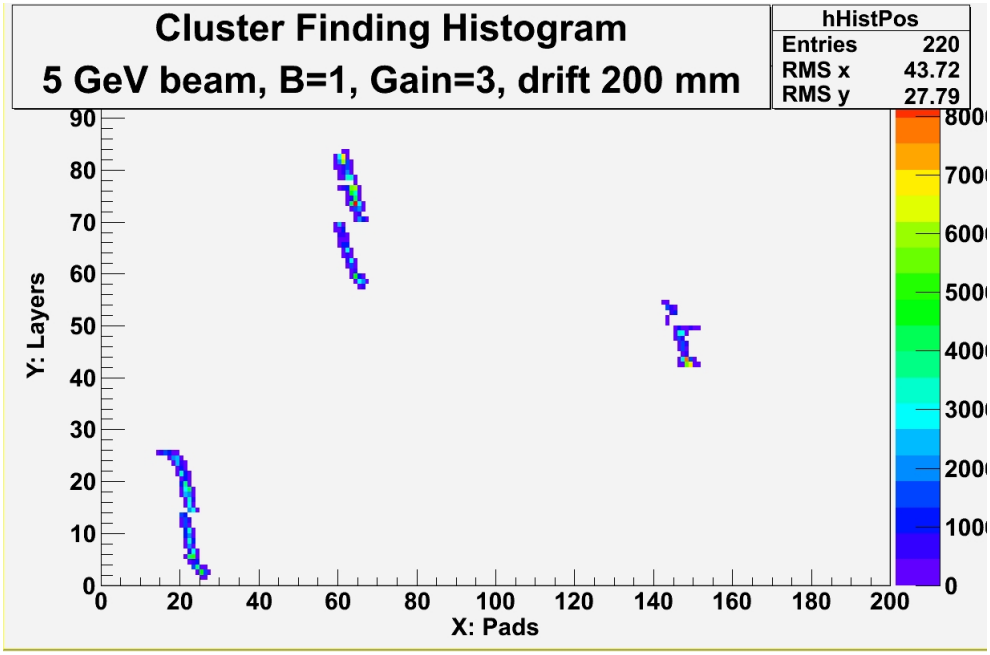

Figure 26: The pad-layer image of the track on which clustering is done.

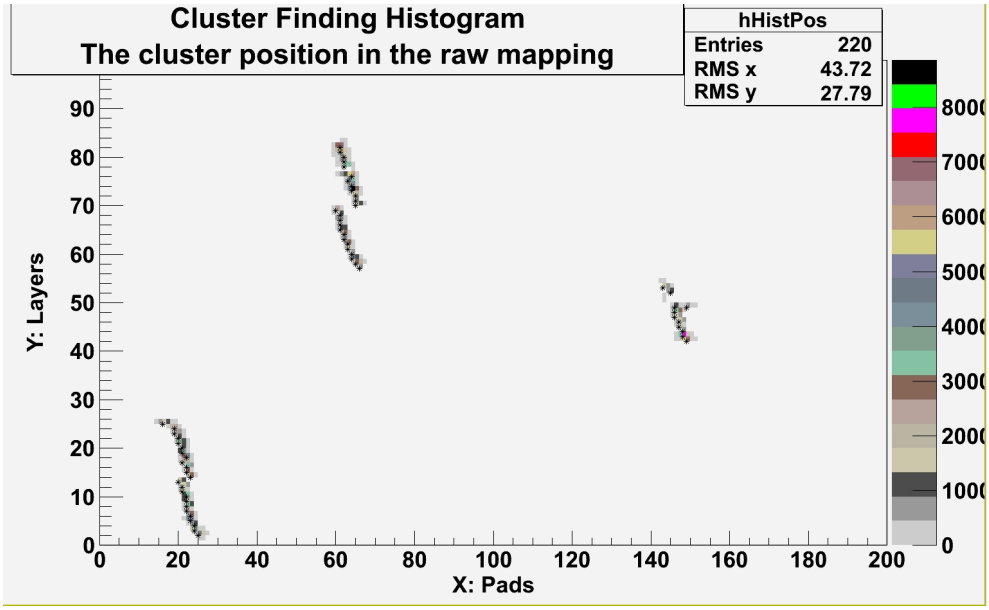

Figure 27: The cluster position in the raw mapping.

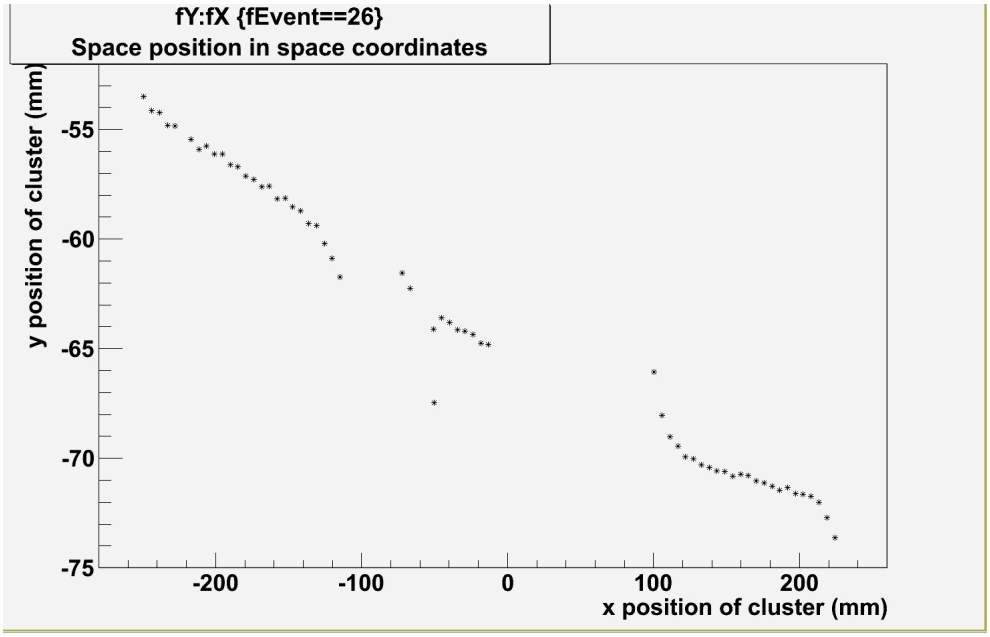

Figure 28: The cluster position in the x-y-coordinate system (space coordinates).

from the weighted mean cluster position to the fitted function, delta Y (often named *residual*), is calculated for the position resolution analysis. The momentum is calculated from the curvature of the fit and both the information about delta Y and the momentum is stored in the Tree.

This procedure is repeated for every event in a run-file.

The number of clusters in each event is plotted in figure 29 for a 5 GeV/c beam. A cut can be made which ignore the events with many clusters, since they probably are events with multiple tracks och delta electrons, which is uninteresting for the analysis.

5.2.2 Results

The reconstructed coordinates shown in figure 30, 31 and 32, where the cluster position in x and y space coordinates are plotted, show that two different problems arises:

The first problem is that there are distortions of the track trajectory at the module edges when B=1 T (known as the "s-shape"). This problem was discovered in the track visualization analysis, and remains a problem in this more accurate tracking analysis. The fact that the distortions at the module edges arise only when the magnetic field is applied, not when the magnetic field is off, makes the reason most likely due to non aligned **E** and **B** fields, i.e. the **B**-field is not parallel to the **E**-field at the module edges. These effects make the electron cloud drift non linear relative to the particle position. If this problem is not solved, the fitted function will be affected and hence the detailed analysis of the position resolution and the momentum determination will be pointless. Since the data is already taken, and there are no possibilities to align the **E** and **B** field with the current experimental setup, the problem must be dealt with in the software. This is the reason for cutting away the problematic areas with the module edge distortions.

The second problem is that there are a systematic error in the weighted mean cluster position

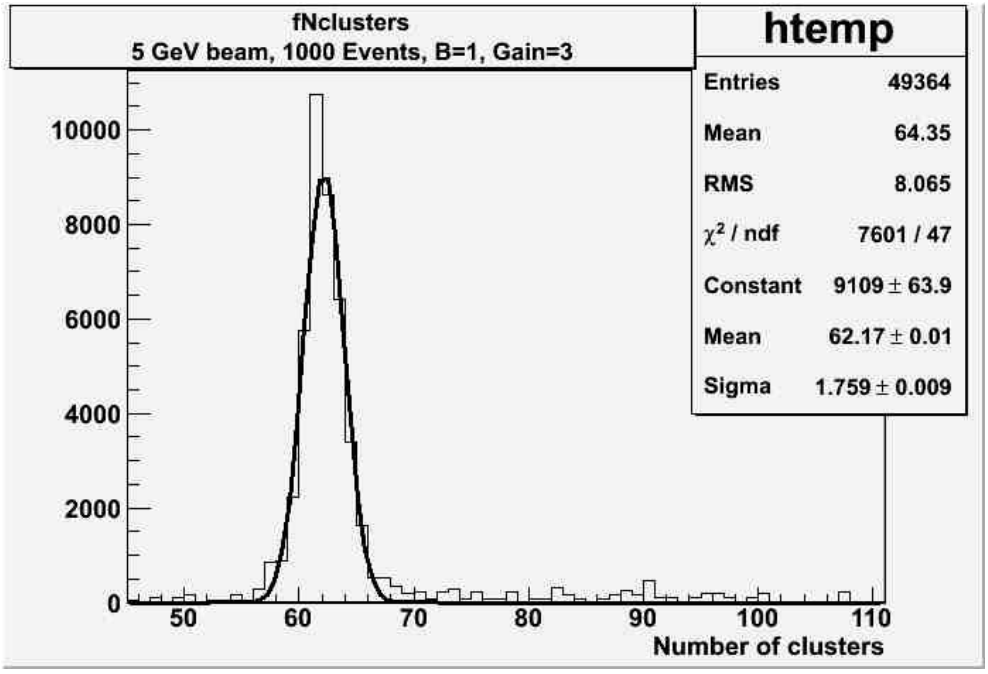

Figure 29: Number of clusters.

relative to the fitted function; the residuals, i.e. the distance from the position of the cluster to the fitted line (delta Y), are consistently above the fitted function on one half of the module, and below the fitted function on the other half of the module. This systematic residual problem arise with both B=1 T and B=0 T T. This problem must also be solved before any detailed analysis of the space point resolution along the full track length can be done. This second problem, called "the systematic residual problem", can be caused by different reasons. It is not caused by the magnetic field, since it is visible with and without the magnetic field, see figure 31 and 32. The pad geometry is complex and can therefore result in mapping problems of the channels to the space coordinate. The most reasonable explanation for this problem is module misalignment relative to each other. The accuracy when mounting the GEM panel in the aluminum frame was not ensured by steering pins but only guided by the accuracy of the screws. Thus translational and rotational inaccuracy between the modules can be an argument for rotating the modules by software. To find the correct way to correct for this problem from tracks is hard and one should need to do a mechanical survey of the mounted GEM structure down to a precision of tens of micrometers. On the present data it remains to limit the study to individual modules in order to get around the problem. Other ILC TPC groups have analyzed only one module.

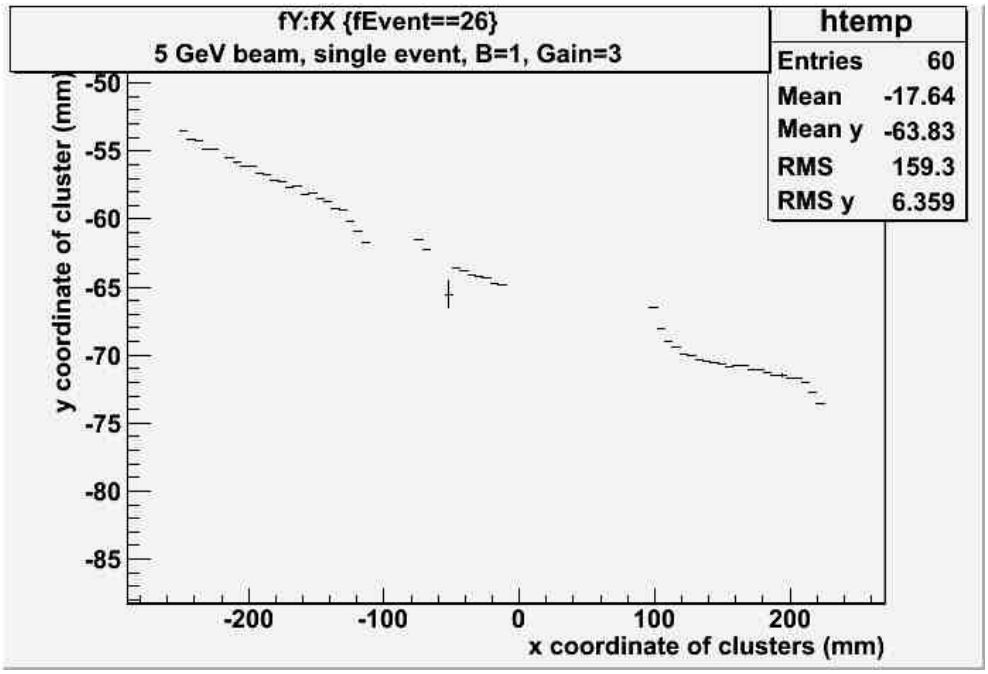

Figure 30: The cluster positions in space coordinates, B=1 T. Module edge distortion due to non aligned magnetic and electric fields are visible (the so called "s-shape").

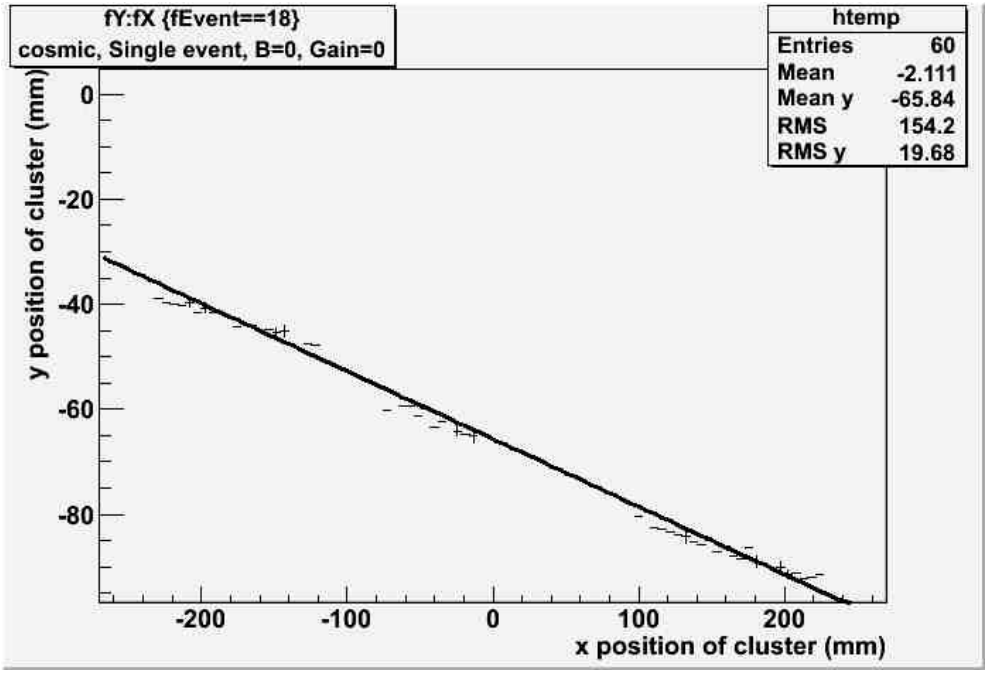

Figure 31: The cluster position in space coordinates. The systematic residual problem is shown, but the module edge distortions does not appear since B=0 T.

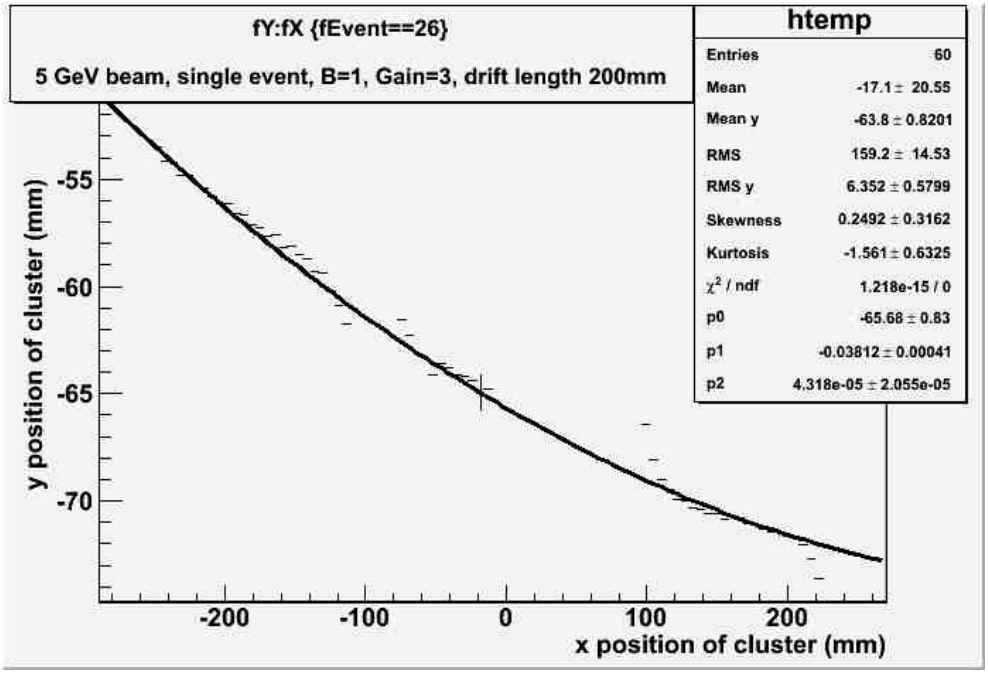

(a) Both the systematic residual problem and the module edge distortions are present.

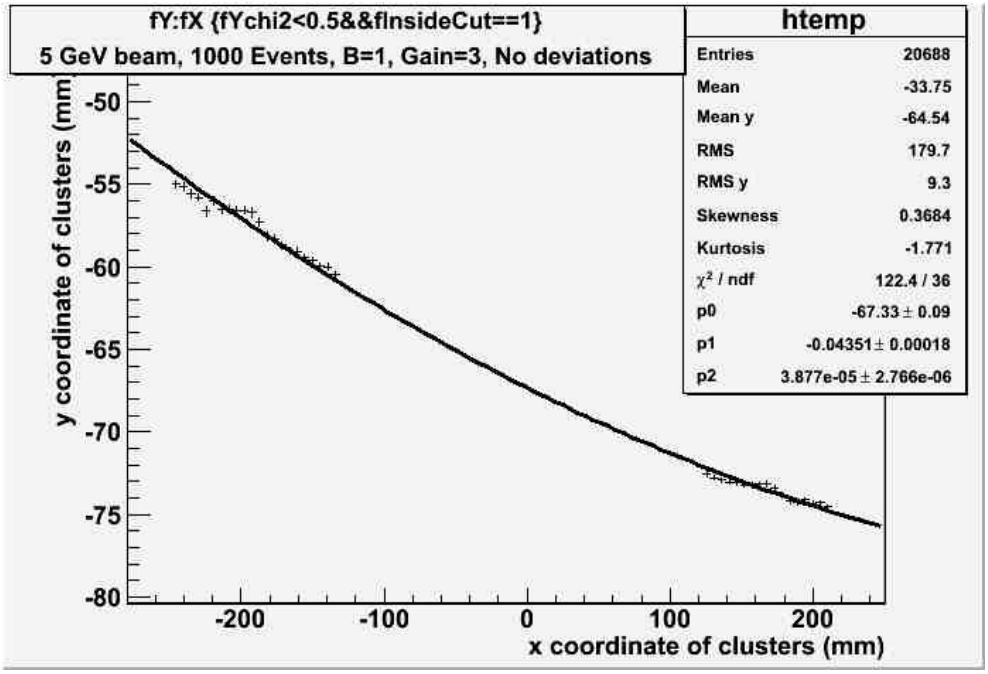

(b) The deviations near the module edges are cut away, the systematic residual problem is still present.

Figure 32: The cluster position in space coordinates. B=1 T, the systematic residual problem shows as the cluster position above resp. below the fitted line.

5.3 Momentum determination

Momentum of the beam during the test was set to 5 GeV/c. The B field was not uniform in the TPC field cage region; the central region was 1 Tesla, but in the outer regions (where module 1 and 6 is located), the magnetic field was considerably lower, which is bad for the momentum calculations until a detailed field map can be used in the analysis. The module edge distortion and the systematic residual problem also contributes to inaccurate determination of the momentum. But on the other hand, a rough estimation of the momentum can be useful for localizing the origin of the problems, and is done here.

The momentum is given by the curvature of the fitted polynomial to the cluster position; we have the following expression for the momentum:

$$p = 0.2998 \cdot B \cdot R[GeV/c]$$

where B is the magnetic field in Tesla and R is the bending radius that the particle describes in the magnetic field [4]. The magnetic field is 1 Tesla and the bending radius is:

$$R^2 = (x - x_0)^2 + (y - y_0)^2$$

where $x_0 = 0$ and $y_0 = R$

$$\begin{gathered} \Rightarrow R^2 = x^2 + (y - R)^2 = x^2 + y^2 - 2Ry + R^2 \\ \Leftrightarrow x^2 + y^2 - 2Ry = 0 \end{gathered}$$

and since $y << R$ we have

$$x^2 - 2Ry = 0 \Leftrightarrow y = \frac{x^2}{2R}$$

which describes the second degree polynomial for the particle track. The coefficient of the second term, k, is thus equal to $\frac{1}{2R}$:

$$\begin{gathered} \frac{1}{2R} = k \Rightarrow R = \frac{1}{2 \cdot c \cdot 1000} \text{ m} \\ \Rightarrow p = \frac{0.2998 \cdot 1}{2000 \cdot k} \text{ GeV/c.} \end{gathered}$$

The reconstructed momentum should be compared to 5 GeV/c, as delivered from the beam. The momentum accuracy of the beam is unfortunately not available.

In figure 33, one can see that the reconstructed momentum has a broad distribution as expected due to the uncertainties in B and errors in the module positions which gives a curvature governed by the position uncertainty and not by the curvature of the track itself. The broad distribution can also be a consequence of the multiple tracks events, whose tracks have lower momenta than the initial beam momentum. A momentum calculation for single modules was done, but the results were not satisfying (although it was a narrower distribution) since the track length is too short for a good analysis of the momentum and in order to obtain any track length at all one must do the analysis on the outer modules, where the magnetic field is the worst. The result from the mean value of the histogram of three module study is $\sim$4.7 GeV/c for both the calculations with and without the module edge distortions.

It seems like the module edge distortions does not make a difference to the momentum resolution since the second degree coefficients are almost the same with and without cuts (the distortions "cancels out"). But as we shall see, it makes a difference for space point resolution.

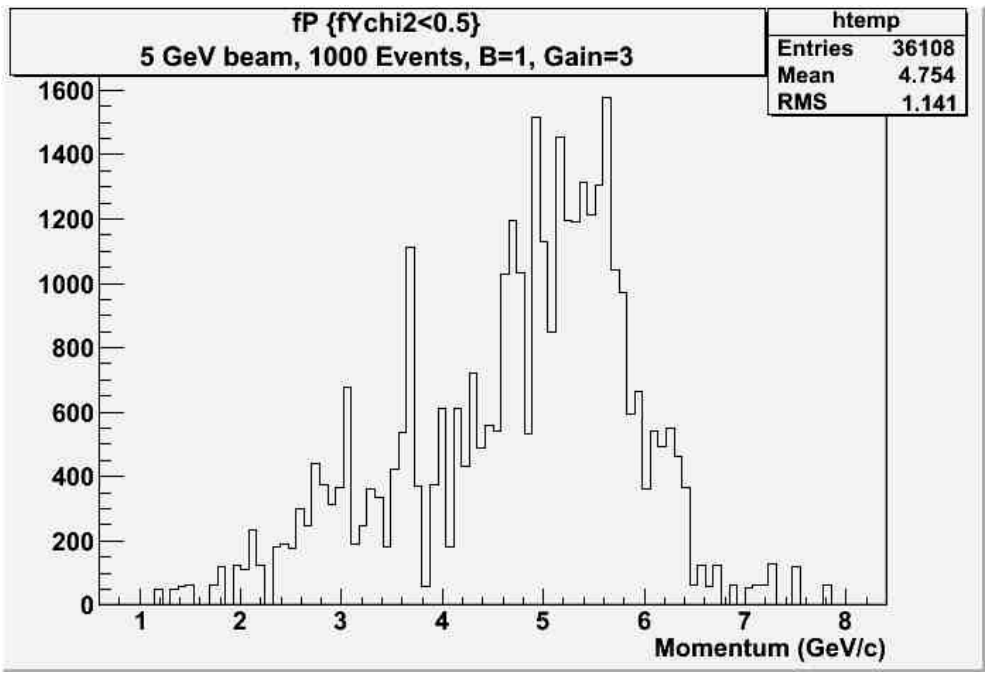

Figure 33: The momentum distribution for a 5 GeV/c beam.

5.4 Position resolution in the bend plane

The position resolution depends on the track angle, the drift length, the pad length and the diffusion that the primary electrons suffers from. The position resolution describes with what accuracy a track coordinate can be determined. Here, we use the fitted function as the true position of the track and relate reconstructed coordinates to the fit in order to find the resolution. From the clusters, the weighted mean position can be calculated and a function is fitted to the points. The position resolution can be calculated as the root mean square (RMS) of the distances (the delta Y, or the *residuals*) of the weighted mean of the cluster to the fitted line. The histogrammed distance of every weighted mean cluster position to the fitted line is a Gaussian distribution and the standard deviation of the fitted Gaussian corresponds to the position resolution. The resolution is determined from the residuals of a *straight line fit* (if B=0 T) or a *second degree polynomial* (if magnetic field is on) to the track coordinates in both pad direction as a function of the drift length. The space point resolution in the final ILC TPC can be determined by extrapolating the fit to the maximum drift length of the ILC TPC. This is important for optimizing the the TPC design parameters for the real ILC TPC detector. As seen from the simulation in figure 5(a), there should be a dependence of the drift distance at 1 T field, while at 4 T field the position resolution should be more or less the same at all drift lengths.

As mentioned before, it is difficult to draw any conclusions from the position resolution analysis for all three modules since the module edge distortions and the systematic residual problem arises. One can though see that the distribution of the distance from fitted line (delta Y) is narrower when cutting off edge deviations due to non parallel magnetic and electric fields, but the systematic residual problem remains. Figure 34 clearly shows the problem. Although dramatic on

this scale, one should remember that these effects are small. The edge effect in figure 34(a) are on a scale of few millimeters, while the systematic residual problem is within ± 0.4 mm. To get rid of this problem, the estimation of the position resolution is restricted to one module, with the edge effects cut away.

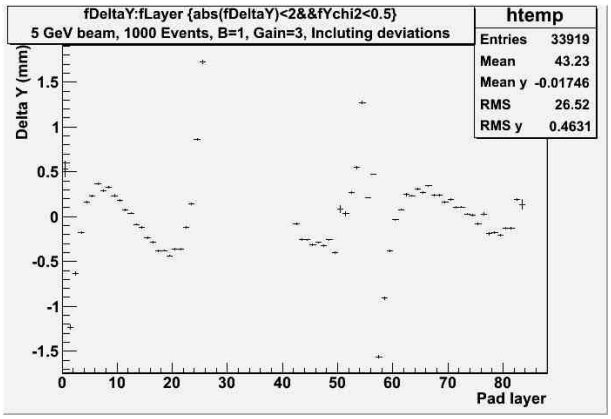

(a) Delta Y including module edge deviations, drift length 200 mm.

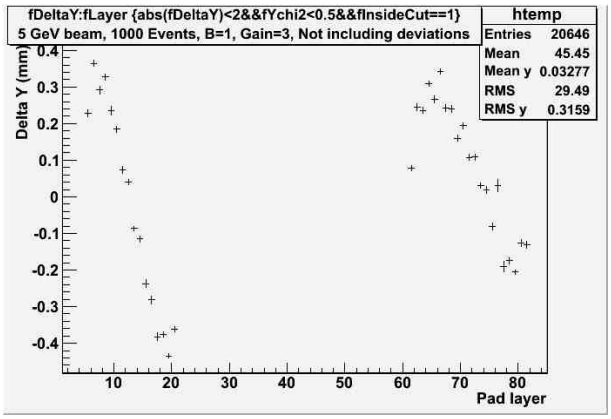

(b) Delta Y not including module edge deviations, drift length 200 mm.

Figure 34: The systematic residual problem.

5.4.1 Single module study of space point resolution

To get around the systematic problems, a single module study is made where the function is fitted only to the cluster position in a single module inside the cut, i.e. without the module edge distortions, see figure 35 and 36. The center module where the lower GEMs does not work is not studied. For the other modules, the result is a position resolution of $\sim$ 120-130 μm.

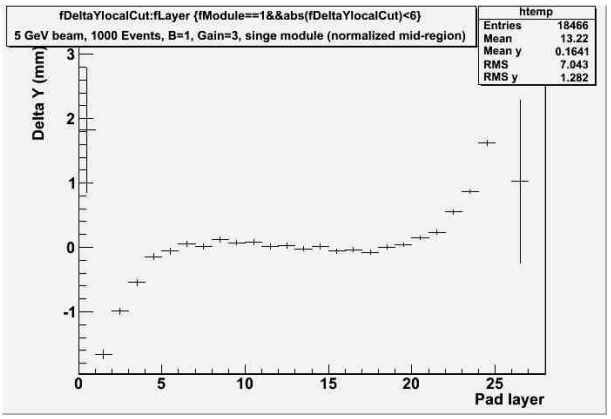

Figure 35: Delta Y in the pad layers for a single module fit, the edge distortions are still visible. B=1 T.

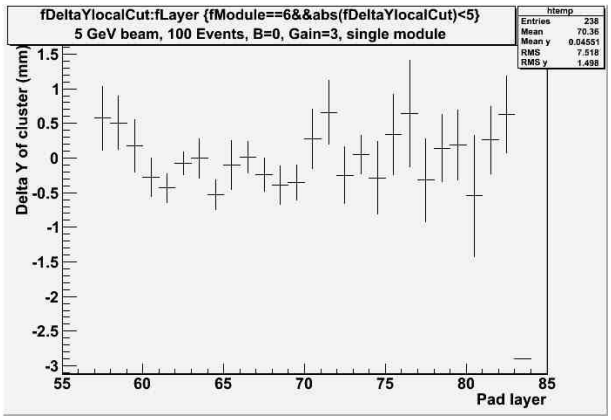

(a) Delta Y inside the cut region - the residuals show a small systematic effects. B=0 T.

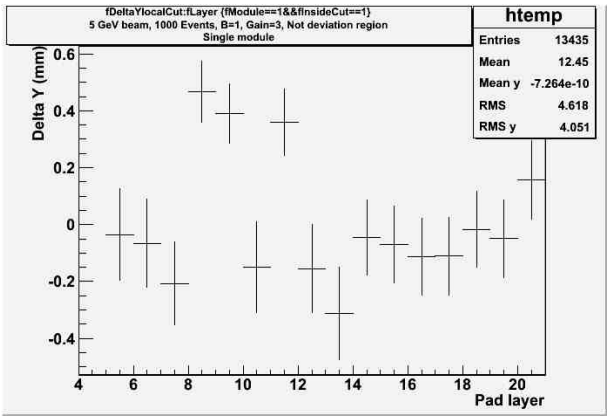

(b) More randomly distributed residuals. B=1 T

Figure 36: The residuals with and without magnetic field, the drift distance is 200 mm.

The position resolution in the bend plane for different drift lengths does not seem to change much. The resolution is $\sim$ 120-130 μm for every run with B=1 T. The expected value is around 100 μm and can be seen in figure 5(a) at page 11. Considering the simulation it seems also understandable that the small difference in drift length from 70 mm to 200 mm does not influence the resolution significantly.

The limited data on no magnetic field runs makes it difficult to analyze these events. But figure 36(a) gives a rough estimation (made on few events) of the position resolution without magnetic fields. The result is, as expected, that the resolution ($\sim 1.5\mu m$, which is in the order of a magnitude worse than with magnetic field) degrades with no magnetic field.

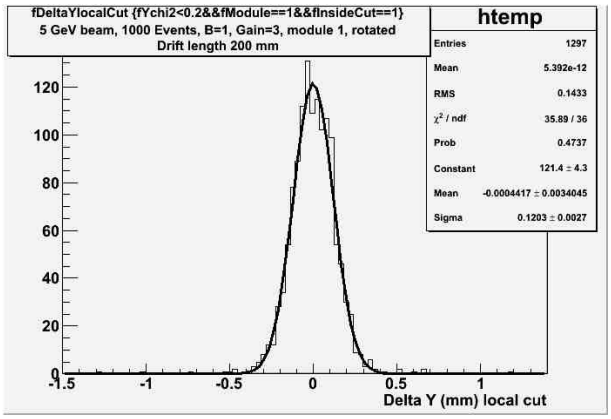

(a) Delta Y for module 1.

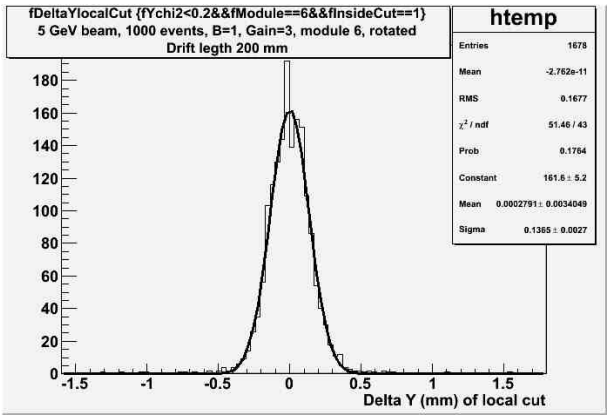

(b) Delta Y for module 6.

Figure 37: Drift length 200 mm.

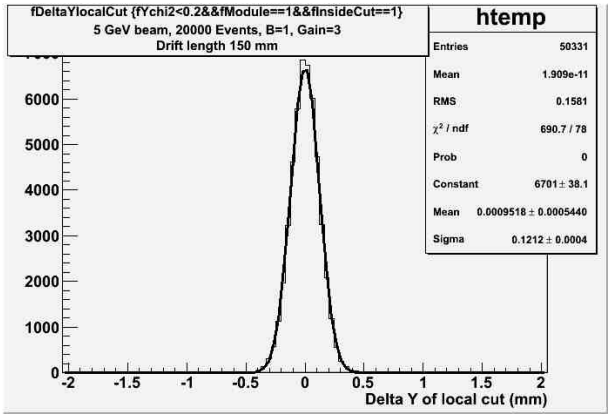

(a) Drift length 150 mm.

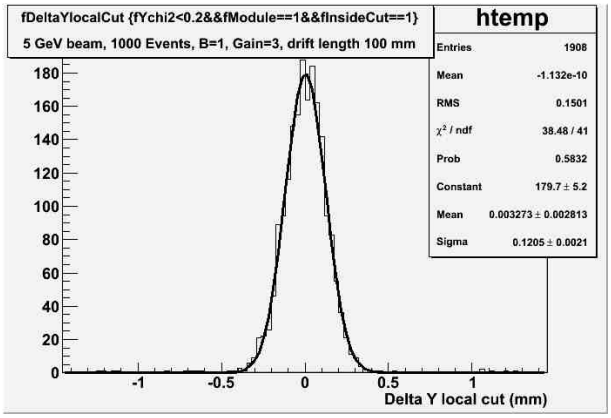

(b) Drift length 100 mm.

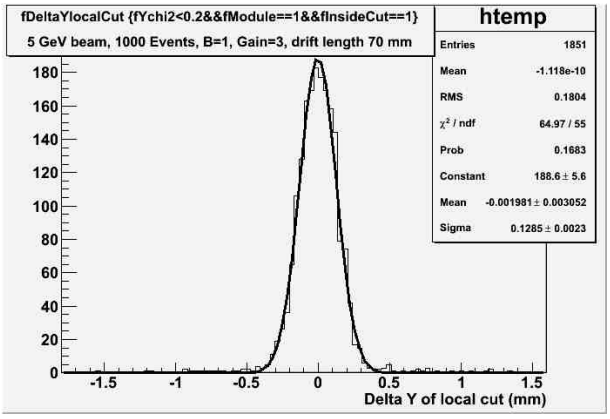

(c) Drift length 70 mm.

Figure 38: Delta Y for different drift distances.

6 Conclusions

The International Linear Collider project is still in its development phase, where it is important to test many design options. One of several detector concepts is the main focus in this thesis, and particular the spatial resolution for the main tracking chamber in the Large Detector Concept, the Time Projection Chamber. A prototype with a newly developed readout system based on Gas Electron Multiplier is tested at DESY and analyzed by (among others) Lund ILC group. Every detail study can be used as input for Monte Carlo simulations, which is important for future studies and the construction of the final TPC. Some problems or considerations that arose during the setup and the analysis were:

1. Distortions at module edges when B=1 T due to E$\times$B effects.

2. Systematic residual problem, probably due to module misalignment.

For higher position resolution, smaller pads or an alternative pad geometry is perhaps needed. But that means that the software has to be more advanced, and the mapping from a channel to a space coordinate is complex. Since the measurements basically confirm the simulations one should expect that the simulated performance at 4 T should be realistic. Unfortunately, the available magnet is limited to 1 T.

The solution to the systematic residual problem was to analyze single modules inside which there no alignment ambiguities since the geometry is engraved into the pad board. The analysis resulted in a position resolution of 120-130 μm compared to the expected 100 μm. Of course, further analysis has to be done with correct module alignment, or alternatively, an accurate known translational and rotational displacement constant. 130 μm can also be improved by increasing the magnetic field from 1 Tesla to 4 Tesla.

Further analysis could be done by estimating the momentum resolution with a simulation. If two tracks are generated; one with exactly known position and momentum, and the other with randomly generated charge distribution values extracted from our measurements done in the test at DESY. From the measurements, we obtained the charge deposited on each pad. Concerning all the involved pads, the charge gives (ideally) a Gaussian distribution, which can be used to generate a random charge value for the simulation. The track will then be reconstructed by the cluster finding- and track reconstruction algorithm described in the analysis section. The result of the simulation is thereby two tracks, the "real" track, and the "measured" track. The measured momentum can be compared to the real momentum and when repeated for many tracks, the momentum resolution can be obtained. It is then straightforward to generalize the simulation to a full size chamber.

7 References

1. K. Ackermanna et al., *Cosmic Ray Tests of the Prototype TPC for the ILC Experiment*, (18 May 2009)
2. J.Baechler, J.C.Berset, T.Christiansson, C.Engster, *FRONT-END ELECTRONICS FOR THE ALICE TPC -DETECTOR*, (CERN, Geneva)
3. Lene Bryngemark, *Exam thesis* (Spring 2009)
4. Richard Fernow, *Introduction to experimental particle physics*, (1986)
5. Dean Karlen, Carleton University, *Investigation of GEM space point resolution for a TPC tracker*,
6. W. R. Leo, *Techniques for nuclear and particle physics experiments*, (1994)
7. Thomas Lohse, Werner Witzeling, European Organization for Nuclear Reserch CERN, *The Time Projection Chamber*, (22 November 1991)
8. Ron Settles, DESY collaboration, *EXTENDED JOINT ECFA/DESY STUDY on PHYSICS and DETECTOR for a LINEAR electron positron COLLIDER*, (March 2004)
9. ALICE TPC Collaboration, *Performance studies with an ALICE TPC prototype*, (7 July 2006)
10. ILC global design effort, *International Linear Collider reference design report - Accelerators*, (August 2007)
11. ILC global design effort, *International Linear Collider reference design report - Detectors*, (August 2007)
12. ILC global design effort, *International Linear Collider reference design report - Summary*, (August 2007)
13. STAR Collaboration, *The STAR Time Projection Chamber: A Unique Tool for Studying High Multiplicity Events at RHIC*, (27 January 2003)
14. Status Report from the LCTPC Collaboration, *TPC R and D for an ILC Detector*, Version No.9 (9 January 1007)
15. http://adweb.desy.de/home/testbeam/WWW/Description.html , (2 July 2009)
16. http://www.linearcollider.org/ , (5 April 2009)

Thanks to:
Lene Bryngemark
Peter Christiansen
Alexander Dobrin
Philippe Gros
Leif Jönsson
Björn Lundberg
Ulf Mjörnmark
Anders Oskarsson
Evert Stenlund
Bozena Wlosinska
And last but not least, thanks to members of the LC TPC teams at Lund, DESY and Japan.